Shaping buildings to promote street ventilation: a large-eddy simulation study

Maider Llaguno-Munitxa[a,b,*], Elie Bou-Zeid[a]

[a] Civil and Environmental Engineering, Princeton University, 41 Olden St, Princeton, NJ 08544, USA
[b] ETH Institute of Technology in Architecture, Stefano-Franscini-Platz 1, Zurich 8093, Switzerland

*Corresponding author at: Civil and Environmental Engineering, Princeton University, 41 Olden St, Princeton, NJ 08544, USA, E-mail address: mllaguno@princeton.edu (M. Llaguno-Munitxa)

Abstract Proper ventilation of urban streets is important for safeguarding the health and comfort of urban inhabitants. To compare the influence of different street canyon building geometries on urban ventilation, large-eddy simulations (LES) have been performed under neutral stability conditions. Five different street canyon building geometries have been tested: the i) flat roof, ii) pitched roof, iii) round roof, iv) terraced building and v) building with balconies. The geometries were configured as seven building arrays, with six street canyons in between them aligned in the span-wise direction. The Air Exchange Rate (ACH) between the street canyons and the free atmosphere has been computed for the different cases. The results show that the ACH is very sensitive to the building geometry; therefore, it appears reasonable to suggest that buildings can be shaped to promote urban ventilation. The paper also proposes an alternative ACH estimation method based on the folded-normal distribution that is shown to produce very good estimates of the LES-computed ACH. The new method uses vertical mean velocity and turbulence statistics that can be obtained from less intensive Computational Fluid Dynamic (CFD) models. A simplified two-reservoir Pollutant Concentration (PC) estimation methodology based on the ACH results is also proposed.

Keywords:

Air Exchange Rate, Air Quality, Architectural Design, Large Eddy Simulation, Urban Ventilation.

1 Introduction

The World Health Organization reported that in 2012, around 7 million people died prematurely – one in eight of the total global deaths – as a result of air pollution. This finding more than doubles previous estimates and confirms that air pollution is now the world's largest single environmental health risk (WHO, 2014). Since adverse air quality tends to be primarily an urban problem, and given the very rapid pace of urbanization in this century (UNFPA, 2014), maintaining good air quality in built areas is of paramount importance to safeguard the health and comfort of urban inhabitants.

Air quality in cities is affected by ambient wind speed and direction, atmospheric stability, solar radiation and anthropogenic pollutant emissions (Britter and Hanna, 2003). Thermal pollution and chemical pollutant concentrations peak in cities, as opposed to the countryside, due to the high and localized anthropogenic emissions, as well as to the topographical and surface material properties of the urban fabric (Landsberg, 1981; Oke, 1987). Luke Howard, a British chemist and meteorologist, was one of the first scientists to address this evidence through observational work in the 1830s (Howard, 1838); and since then, research on urban air pollution has been on-going. In the second half of the 20th century, the first comprehensive air quality policy was established in the UK - the Clean Air Act of 1956 - which was followed by the US clean air act in 1963. Of specific relevance to urban pollution, an effort to move polluting plants and manufacturing outside of cities has been underway for decades. Vehicle circulation restrictions are also being implemented in various cities. That is the case for Madrid, for example, with the newly approved anticontamination protocol, or London, with the Low Emissions Zone (LEZ) regulation established in 2008 (Transport of London, 2015). Similar policies are concomitantly being implemented in other cities around Europe such as Paris, Milan or Budapest.

Nevertheless, since emissions are not the only factor contributing to pollution risk, regulations that pertain to urban planning and architectural design considerations are also starting to be implemented. The Hong Kong Air Ventilation Assessment (AVA) is one such regulation formulated to assess the impact of architectural designs on the pedestrian wind environment (Ng, 2009; Ng, 2012). Such building design guidelines that promote urban ventilation by accelerating pedestrian-level air flow and pollutant dispersion are becoming increasingly more important. This is especially true for dense urban environments where urban ventilation is most compromised (Oke, 1988b). However, despite Hong Kong's example, urban policies that incorporate guidelines to promote urban ventilation are still scarce. The reasons for this are numerous; one of the most important being the barrier posed by the technical expertise and effort required for modelling of air flow and pollutant dispersion that many local administrations do not possess to tailor regulations for their cities. This is why architectural and urban planning processes often fail to incorporate design strategies to enhance urban ventilation (Oke, 1988a). Therefore, the definition of broad design guidelines and urban ventilation estimation strategies that are of wide applicability across many cities would be most useful for an easier implementation of urban ventilation criteria within planning and architectural design processes.

While urban structures differ among different cities as well as between different neighbourhoods within the same city, arguably one of the most characteristic world-wide urban typology is the urban street canyon. The urban street canyon, is a typological urban configuration in which the dominant sources of pollution, vehicle emissions, concentrate in close proximity to the pedestrians (Britter and Hanna, 2003). Therefore, the urban street canyon has been often studied as an archetypal model in the context of urban air quality, urban ventilation, and urban heat island investigations, with the aim of developing a universal understanding of these problems that is of wide applicability.

Within an urban street canyon, the presence of dominant circulation patterns and the turbulent momentum and scalar exchanges between the inside and the outside region of the canyon are very important aspects to take into account for dispersion calculations. For high building height (H) to street width (W) ratios, a particularly adverse flow regime could occur where the flow above the canyon skims across with minimal exchanges with the air inside the canyon (skimming flow regime, (Oke, 1988b)). That is, for street canyons with a wind angle nearly perpendicular to the main axis of the canyon, when the building spacing is reduced beyond a certain threshold, a decoupling of the flows above and below the canyon occurs. One way to quantify these exchanges is via a street canyon transfer velocity U_e, induced by mean (including dispersive) and turbulent fluxes; this transfer velocity has been extensively studied both experimentally and numerically (Vardoulakis et al., 2003). For air quality applications (or urban heat), the exchange velocity is best defined through the average rate of mass (or heat) transfer in or out of the urban canopy layer at a horizontal plane of interface between the in-canopy and above-canopy flows. Britter and Hanna (2003) introduced the concept of exchange velocity for the first time and studied the spatial temperature distribution and scalar exchanges at the plane of interface, to conclude that U_e was approximately 1% of the characteristic wind velocity U_{ref} above the street canyon. U_e is also frequently used in numerical simulations (e.g. Hamlyn and Britter, 2005; Solazzo and Britter, 2007). Di Sabatino et al. (2007) and Di Sabatino et al. (2008) used the exchange velocity to compare the performance of the k-ε turbulence closure model and the advection-diffusion method. Hamlyn and Britter (2005) estimated U_e as a fraction of U_{ref} and found that it ranges from 0.3% to 1% for regular cube arrays with variable packing densities. Solazzo and Britter (2007), through numerical studies, applied the concept of U_e to a street canyon with weak buoyancy effect, and concluded that the temperature inside the street canyon is nearly uniform and that U_e is about 1% of the free-stream wind speed.

Estimations of exchange velocities were also performed through experimental work. Barlow and Belcher (2002) and Barlow et al. (2004) developed wind tunnel experiments using the Naphthalene sublimation technique. In their analysis, they used the concept of a transfer velocity to relate the flux out of the canyon to the concentration within it and reported that the transfer velocity to wind speed aloft ratio varies with the building aspect ratio, reaching a maximum in the wake interference regime. This regime occurs in street canyons with $0.3 < H/W < 0.65$ (i.e. more widely spaced than the skimming regime) and is characterized by stronger vertical exchanges and interactions of the wakes of distinct buildings. Salizzoni et al. (2009) estimated the exchange velocity between the canyon and the external flow by measuring the cavity wash-out time, that is, the time it takes for the whole air cavity volume of the street canyon to be removed from the street canyon, and addressed the influence of the external turbulence on the transfer process. Salizzoni et al. (2011) developed wind tunnel experiments using the PIV technique and concluded that turbulent transfer is due to the coupling between the instabilities generated in the shear layer above the canyons and the advected turbulent structures in the outer boundary layer (the air above the urban boundary layer), and proposed to estimate the mass exchange between a two-dimensional cavity and the overlying boundary layer by looking at the pollutant wash-out from the cavity.

The exchange velocity has also been used for the so called "city breathability" concept that was introduced by Neophytou and Britter (2005) to express the potential of a city to remove pollutant and heat entrapment from urban environments. The same urban breathability ventilation indicator was used, among others, by (Buccolieri et al., 2010; Panagiotou et al., 2013; Tominaga, 2012). Panagiotou et al. (2013) quantified city breathability using U_e and conducted Reynolds-Averaged Navier Stokes (RANS) simulations for an inhomogeneous urban area to conclude that urban morphologies determine the shape and size of vortical structures that are present in the flow field, and thereby the exchange processes with the flow above. However the studies developed did not systematically study the effect of building morphology. Buccolieri et al. (2015), also through RANS simulation, studied city breathability by combining two ventilation concepts: mean flow rate and age of air. They developed studies of aligned arrays of cubes with variable areal building densities and concluded that the local mean age of air increases substantially by increasing the density. A similar strategy was followed by Ramponi et al. (2015) who looked at the ventilation performance of street canyons by means of the local mean age of air. As described by Ramponi et al. (2015) the local mean age of air (τ_p) is a statistical measure of the time it takes for a parcel of air to reach a given point in the flow field after entering this flow field. That is, for urban wind flow, it can be defined as the average time it takes for the external "fresh" air parcel that enters into the street canyon to then exit that canyon (Hang et al., 2009).

Another frequently used ventilation indicator is the Air Exchange Rate (ACH), that is, the volumetric air exchange between the street canyon and free atmosphere per unit time (Liu et al., 2005). Liu et al. (2005), Riain et al. (1998), making use of LES, investigated the concept of air exchange rate (ACH), pollutant exchange rate, average pollutant concentration, and pollutant retention time, to quantify the street canyon ventilation and pollutant removal performance. Xie et al. (2006) developed numerical studies to investigate the effect of solar radiation on the ACH of an idealized street canyon and reported that the air exchange rate $ACH_{w'}$ induced by the vertical velocity fluctuation w' is generally larger than ACH_w induced by the mean vertical velocity $\overline{w}$.

Since LES requires high computational resources, Li et al. (2005) estimated ACH using the more cost-effective RANS technique, by assuming isotropic turbulence at the top of the canyon. Their

RANS model used a k-ε closure, and hence this isotropy assumption was needed to infer the vertical velocity variance from the computed turbulent kinetic energy (TKE). The RANS ACH was reported to produce a slight over prediction of the LES ACH, with a deviation within 20% . These studies were followed by Cheng et al. (2009) who also used RANS with a k-ε turbulence closure to study street canyon ventilation & pollutant removal under various heating configurations & building geometries. A similar approach was followed by Moonen et al. (2011) who introduced the concept of Ventilation Potential (VP) and developed RANS and LES studies of various street canyon and courtyard building geometries with variable angles of attack (angle between the street canyon axis and the wind direction). The ventilation potential in that study was described as a statistical measure to assess the removal of scalars and was defined by using the magnitude of the flux through the plane of interface, normalized by the free-stream wind speed and parameterized as a function of the courtyard's length-to-width ratio and of the angle of attack of the incoming wind flow.

In these previous studies, various ventilation indicators (one should point out however that all these indicators are correlated) have been utilized to assess the influence of parameters such as building aspect ratios, incoming inflow turbulence characteristics, or angles of attack on the street canyon urban ventilation. In cases when computationally less demanding approaches for the computation of street ventilation have been sought, a RANS approach was selected. Some of these prior studies that have used RANS models for the computation of street ventilation have reported results to be within a reasonable uncertainty range in comparison to experimental or LES results. However, given the inherent limitations of RANS models where all turbulent fluxes (the full spectrum) need to be parameterized, the general validity of RANS to estimate the ventilation potential of urban street canyons remains in question. RANS in general is particularly challenged by complex geometries, similar to the ones we simulate here as presented later, where intricate flow separation behaviour might occur (Slotnick et al., 2014). Given these limitations and the fact that RANS models do not account for turbulent transport in a direct manner, they are not ideal to calculate the air ventilation and pollutant dilution rates. LES on the other hand captures the transport produced from a broader spectrum of scales, namely the large eddies that in fact are the most important for canyon exchanges. LES explicitly calculates the resolved-scale turbulent transport and models only small subgrid-scale processes. Therefore, LES is the tool of choice for determining ventilation rates. Thus, for the street ventilation studies presented in this paper, the LES technique has been utilized.

Another important aspect to take into account is that prior literature has mainly focused on the study of 'box like' idealized building geometries disregarding the influence of further architectural scale geometrical variations in street ventilation. That is, the morphological parameters of urban street canyons have been generally reduced to the plan area λ_T and frontal area λ_F densities. The total building plan area, A_P, and the total building frontal area, A_F , in a total built lot of area, A_T, can be used to define the "lambda parameters": the areal or planar density being $\lambda_P = A_P / A_T$ and the frontal area density $\lambda_F = A_F / A_T$ (Britter and Hanna, 2003). To a lesser extent, the influence of the building streamwise length (W) to height ratio, as well as the influence of the angle of attack of the wind flow relative to the main street axis, have also been researched. However, the majority of this literature investigated cuboid building shapes, i.e. flat roofs. Only a limited number of prior studies have looked at more complex street canyon building geometries, such as pitched roof configurations. Notably, these investigations have found architectural geometrical variations to have a strong influence on the street canyon air flow dynamics. Rafailidis (1997) and Rafailidis and Schatzmann (1996) developed wind tunnel studies to investigate the influence of pitched roof building arrays on street flow and pollutant dispersion and concluded that altering the roof geometry can have bigger impact on urban air quality than modifying canyon aspect ratios. These investigations were followed by (Dezső-Weidinger et al., 2003; Huang et al., 2009; Kastner-Klein et al., 2004; Kastner-Klein and Plate, 1999; Kellnerova et al., 2012; Takano and Moonen, 2013; Theodoridis and Moussiopoulos, 2000; Xie et al., 2005; Yassin, 2011) who through wind tunnel and numerical studies, highlighted the role of roof geometry on street canyon air flow and turbulence statistics.

However, the main focus of these papers was not the estimation of urban ventilation. Therefore, the effect of architectural considerations such as variable roof designs on urban ventilation remains poorly understood. Furthermore, the impact of further architectural and street level features, such as those depicted in (Fig. 1), on street ventilation is yet to be researched. These knowledge gaps motivate this study, which aims to advance our understanding of urban ventilation by considering the ACH of various street canyon geometries with variable façade and roof geometries. A suite of LES cases is modelled to compute the air exchange rate for street canyon morphologies with variable roof and façade configurations. The research complements the experimental and LES results presented by Llaguno-Munitxa et al. (2017), where the focus was on validating the LES and investigating the mean and turbulence statistics of the different geometries. Further LES cases have been performed for this paper to compute the ACH of five variations on building geometry, as detailed in the next section.

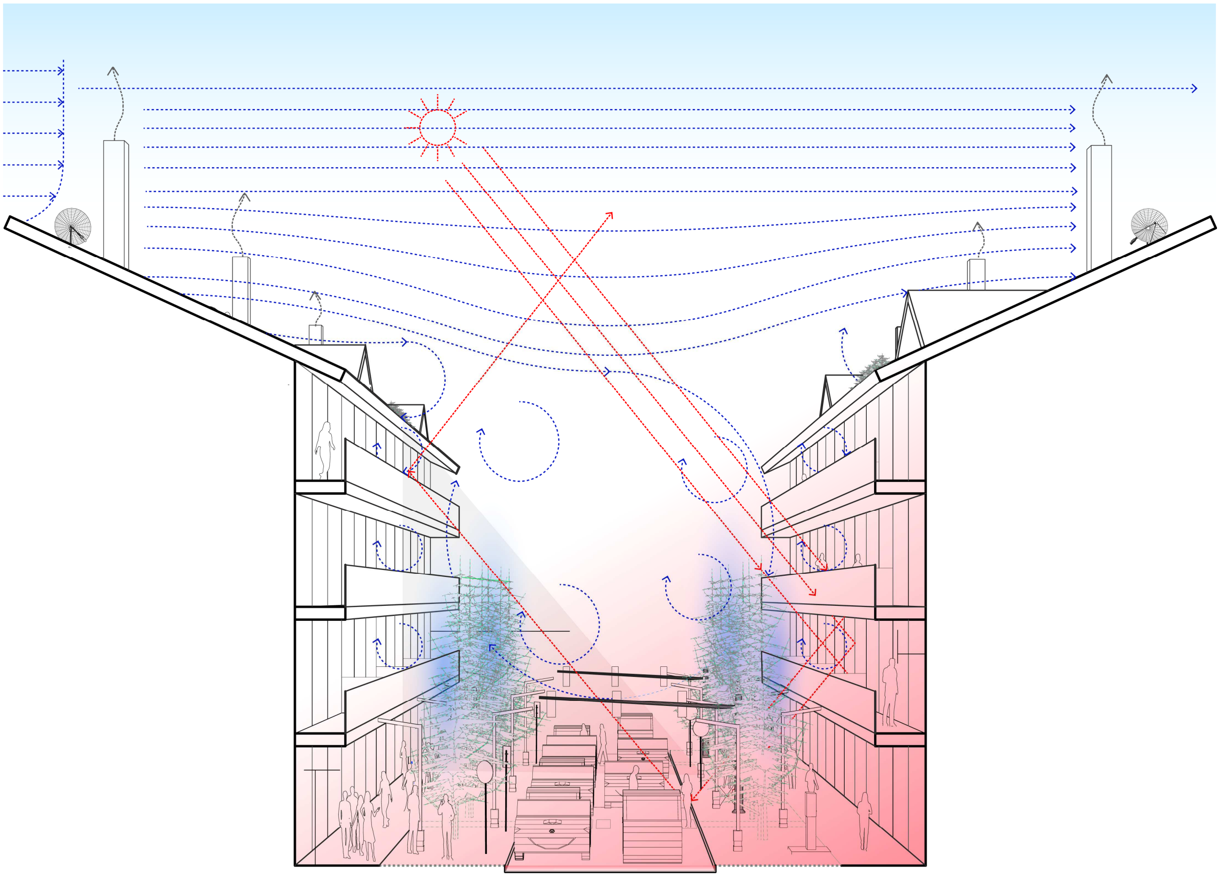

Fig. 1 Illustrative figure to show a typical urban canyon scenario. Pollutants emitted by vehicles and chimneys, and the entrapment of thermal pollution are illustrated to show their dependence on urban furniture and local architecture.

Specifically, the driving questions of this paper are: 1) How does roof and façade geometry influence air exchange between a canyon and the air aloft? 2) How can this exchange rate be accurately parameterized in the absence of the direct measurements allowed by LES (from the mean velocity and TKE available through RANS for example)? How does the street level concentration of a pollutant depend on the emission rate of that pollutant, its concentration above the street canyon, and urban geometry? The details of the simulations are presented in the following two sections, and the results are analysed and reported in section 4. A summary and conclusions are included in section 5.

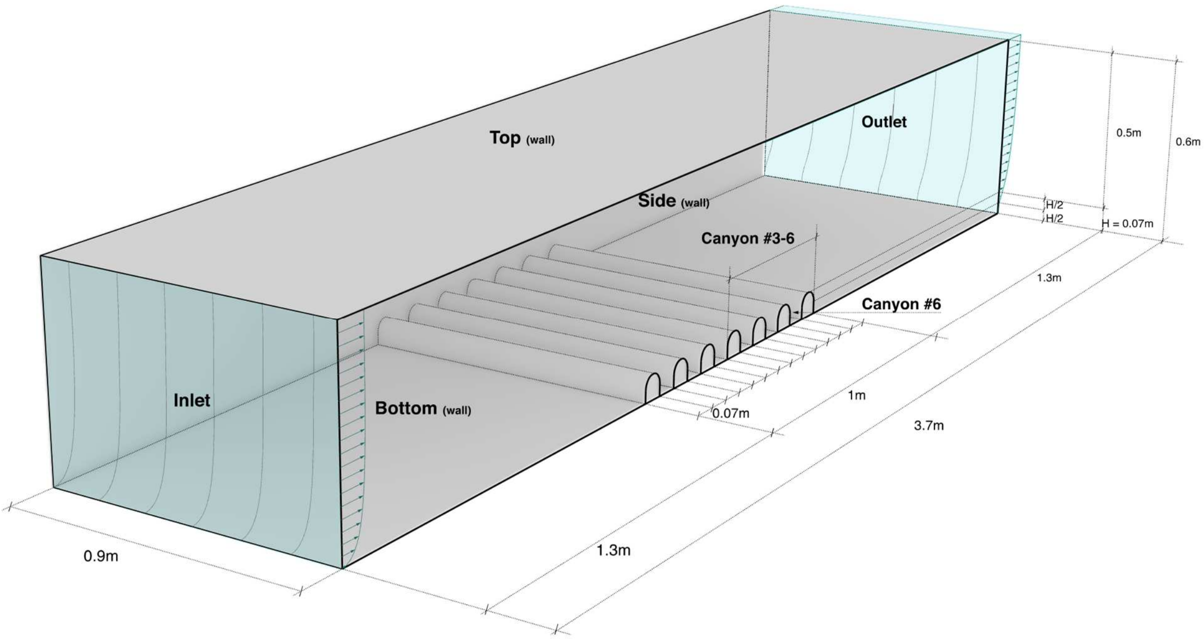

Fig. 2 A schematic of the LES computational domain.

2 Building Geometries

The computational domain is nominally 3.724 m long, 0.912 m wide and 0.608 m tall, and the top, bottom, and side walls have been specified as hydrodynamically smooth wall boundaries mimicking the cross section of the wind tunnel that was used to validate the LES code (Llaguno-Munitxa et al., 2017). An underlying assumption is that the Reynolds number (*Re*) is sufficiently elevated such that the results are not strongly dependent on the length scales used in the problem. This assumption was investigated in Llaguno-Munitxa et al. (2017) and found to be acceptable, though continued dependence on *Re* was noted since the code used (Fluent) does not discard the viscous term as many codes used for atmospheric simulations do. Seven building arrays have been positioned perpendicular to the approach flow and thus the resulting six street canyons are aligned in the span wise direction (see Fig 2). In order to guarantee a fully developed wind profile, the measurements and simulation data analysis have been conducted in Canyon#06, the last downstream canyon. Figure (3) shows the vertical profiles of mean velocity for the central axis for one of the tested geometries, the round roof, obtained with two different inflows (that we will detail shortly) to confirm that the results from the last one are indeed representative of a fully developed (i.e. infinite) array and not strongly dependent on the inflow. These results coincide with those obtained by Brown et al. (2000) who developed wind tunnel studies composed of a similar seven-building array configuration, and who reported that only after canyon #3 or #4 can the flow be considered "in equilibrium" or fully developed.

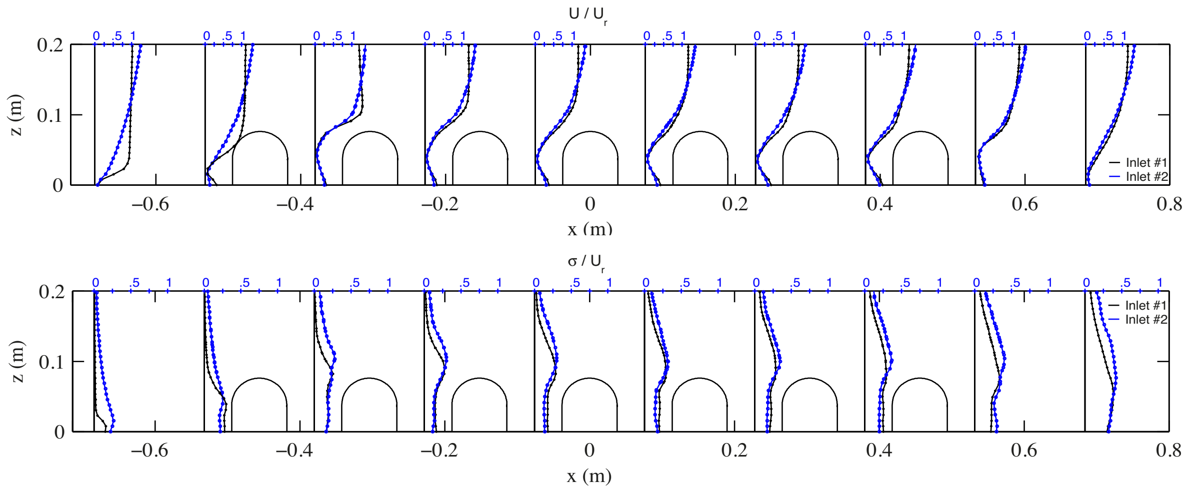

Fig 3 The top figure displays the normalized mean velocity magnitude for the round roof geometry for the central axis of all 6 canyons (flow is from left to right). The bottom figure displays the total root mean square (rms) velocity σ_t for the central axis of all 6 canyons. Two inlet conditions are displayed (inlet #1 and inlet #2) as will be described in Section #3.

An aspect ratio of S/H = 1 has been defined for the street canyons (where S is the spacing between the buildings and H is their maximum height (the vertex for non-flat roofs). In the simulations, we use $S = H = 0.07$ m. The vortex circulation that is created in street canyons oriented perpendicular to the approach flow has been described in prior publications (e.g. (Hunter et al., 1990). The angle of attack has been constrained to 90º in the present simulations, representing canyons that are perpendicular to the mean wind. The frontal area density λ_F and the plan area density λ_P (Britter and Hanna, 2003) have been kept constant and the atmospheric stability is neutral in all simulations since we aim to strictly focus on the influence of the architectural scale geometrical features. The building geometries that have been studied are: i) the flat roof ii) the pitched roof, iii) the round roof, iv) the terraced building and v) building with façade balconies.

3 Numerical setup

Large-eddy simulations have been performed for the 5 studied building geometries. As opposed to RANS models, LES directly calculates the large-scale turbulent structures (larger than the grid or filter scale) and only requires modelling of the smaller scales. This is one of the main reasons why LES is at present the most appropriate tool for determining ventilation rates (at realistic *Re*) and has become widely used for turbulent flow simulation in engineering and environmental applications, including for urban flows (Anderson et al., 2015; Bou-Zeid et al., 2009; Giometto et al., 2016; Inagaki et al., 2012; Li et al., 2016; Nazarian et al., 2017; Xie and Castro, 2009; Yaghoobian et al., 2014). Here we use the LES solver of Ansys Fluent 14.5. The filtered LES continuity and momentum equations solved by Fluent LES reduce for incompressible neutral flow to:

$$\frac{\partial \tilde{u}_i}{\partial x_i} = 0, \tag{1}$$

$$\frac{\partial \tilde{u}_i}{\partial t} + \frac{\partial}{\partial x_j}\left(\tilde{u}_i \tilde{u}_j\right) = -\frac{1}{\rho}\frac{\partial \tilde{p}}{\partial x_i} + 2\nu \frac{\partial \tilde{S}_{ij}}{\partial x_j} - \frac{\partial \tau_{ij}}{\partial x_j}. \tag{2}$$

The tilde (˜) here denotes filtering; p is the pressure; u_i the velocity vector; x_i the position vector; S_{ij} is the strain rate tensor; τ_{ij} is the subgrid scale (SGS) stress tensor; ν is molecular viscosity; and ρ is the fluid density. The deviatoric part of τ_{ij} is modelled in Fluent via an eddy viscosity closure ($\tau_{ij}^{D} = -2\nu_t S_{ij}$), while the isotropic part is added to the pressure as is common in many LES codes (see for example Bou-Zeid (2005)) . The Algebraic Wall-Modelled LES (WMLES) SGS model has been used in the numerical experiments. WMLES is a hybrid RANS/LES method (RANS is used in the regions where the turbulence is in equilibrium and LES is used where non-equilibrium occurs). Through this approach, the need to resolve the viscous sublayer is relaxed (wall-resolved LES, see Pope (2000)) and the computational cost of the simulations is substantially reduced. The SGS eddy viscosity ν_t in WMLES is calculated through the formulation of Shur et al., (2008). This formulation combines a mixing length model for the RANS region, a modified Smagorinsky model (Smagorinsky, 1963) for the LES region, and the wall damping function of (Piomelli et al., 1988). The resulting expression of ν_t hence features a hybrid mixing length scale (ANSYS 2013):

$$\nu_t = \min\left[\left(\kappa d_w\right)^2, \left(C_{smag}\Delta\right)^2\right]\bar{S}\left(1-\exp\left|-\left(\frac{y^+}{25}\right)^3\right|\right). \tag{3}$$

Here, d_w is the distance to the wall; S is the strain rate magnitude; κ = 0.41 is the von Kármán constant; C_{Smag} = 0.2 is the Smagorinsky model constant; and y^+ is the distance normal to the wall in viscous units. This LES model uses a modified grid filter scale to account for the grid anisotropies in wall-modelled flows:

$$\Delta = \min\left(\max\left(C_w d_w; C_w h_{\max}; h_{wn}\right); h_{\max}\right), \tag{4}$$

where, h_{max} is the maximum length of the cell's edge, h_{wn} the wall-normal grid spacing, and C_w = 0.15 a constant.

The SIMPLEC scheme is used for the pressure-velocity coupling. The spatial discretization for the momentum equation uses the Least Squares Cell based method for the gradient, standard method for the pressure, and bounded central differencing for the momentum. An implicit second-order scheme is used for the time advancement. The dimensional time step size has been set to dt = 0.00025 s. The cases have been run for 60,000 time-steps. The eddy turnover time is ~ 0.0422 s due to the small spatial scale of the model (see table 2); therefore, each simulation includes about 355 eddy turnovers, which is sufficient for the statistics to converge. The time-step ensures that the Courant–Friedrichs–Levy (CFL) number is always smaller than 1 ($\approx$ 0.06) at all grid points. The initial 40,000 time-steps were not considered in the calculations to remove the influence of the initial conditions, hence the results shown are averaged over the last 20,000 time steps, equivalent to about 120 eddy turnovers (about 5 seconds in physical time).

The simulation has been set so that it provides a sufficient degree of similarity with a typical urban-like street canyon environment, though the length scale of the model building was reduced to L_m = 0.07m for the validations against wind tunnel experiments reported in (Llaguno-Munitxa et al., 2017). An equivalent real world prototype would have a characteristic length scale of L_{ref} = 15 m (typical street canyon building height), and a typical urban characteristic velocity of U_{ref} = 2 ms^{-1}. Therefore, the studied length scale ratio L_m/L_p between the model and the real building is ≈ 1/200. The LES simulations have been conducted at U_r = 1.8 m s^{-1} , the upstream incoming air velocity at 2H, corresponding to a Reynolds number $Re_M = 9.12\times10^3$, based on the 0.07m length scale of the buildings and an air viscosity of 1.5×10^{-5} m^2 s^{-1}. Given the scale differences between the model and the prototype, the required velocities to be achieved to meet dynamic similarity (match *Re*) were not reproducible in the wind tunnel as described in (Llaguno-Munitxa et al., 2017), and subsequently they were not reproduced in all numerical simulations. *Re* will have some quantitative impacts on the results, especially so for the round roof geometry case, that were assessed by conducting simulations at an $Re \approx 2 \times 10^6$ that is closer to typical real-world values (see Llaguno-Munitxa et al., (2017)). The broad conclusion from that study is that the impact of geometry on urban ventilation will not be drastically influenced by the *Re* (Llaguno-Munitxa et al., 2017), and thus geometries can be compared for their ventilation potential using the smaller domain simulation we already conducted (although quantitative results will be sensitive to *Re*). Given these findings, and given the variability of *Re* in various real-world applications, we focus here on the larger number of simulations performed at the same *Re* as, and validated against, our previous wind tunnel studies.

A grid with hexahedral cells is employed in the three-dimensional domains. Grid sensitivity studies were performed for the computational mesh and a grid cell resolution of 0.007×0.007×0.007 m has been adopted. The exact number of grid nodes varied between geometries, but it was ≈ 4.75×10^6 nodes with ≈ 80×120×490 spanning the *z*, *y*, and *x* directions, respectively. A distance of 1.308 m was left between the first street canyon model and the inlet of the domain and from the last canyon model to the outlet, mimicking the wind tunnel. The essential simulation parameters are summarized in Table 1.

Table 1. Numerical set-up parameters

Front/top area density	λ_p λ_t = 0.076 m
Inlet velocity	U_r = 1.8 ms^{-1}
Local grid scale	Δ = 0.0076 m

Flow time across full domain	$T_{FD} = L\ U_r^{-1} = 2.06$ s
Time computed	$T_c = 5$ s
Building-scale eddy turnover time	$T_{T0} \approx H\ U_r^{-1} = 0.0422$ s

The outlet has been specified as a zero-gradient boundary to generate a fully developed flow. For the inlet, a mean logarithmic velocity profile with a fluctuating velocity generated using the so-called "Vortex Method", which generates a time-dependent inlet condition through the introduction of a random 2D vortex as detailed in Fluent theory guideline (ANSYS 2013), has been used with 190 vortices. The turbulent intensity has been set to 5% and the turbulent to molecular viscosity ratio to 10. The log law mean profile simply follows the classic formulation:

$$u_z = \frac{u_*}{k}\left[\ln\left(\frac{z-d}{z_0}\right)\right], \tag{5}$$

where the upwind terrain roughness is set to $z_0 = 0.03$ m, the friction velocity to $u_* = 0.34$ ms^{-1}, and the displacement height to $d = 0.03$ m. This results in an inlet profile that has significant shear at the scale of the building, mimicking inflow from other buildings upwind. The same inlet conditions (called *Inlet #2*) have been applied to all studied building geometries. More details on the numerical setup can be found in Llaguno-Munitxa et al. (2017).

The simulations were also performed with a laminar inlet and a homogeneous flow profile (called *Inlet #1*). Fig. 3 displays the results obtained with the two different inlet conditions. *Inlet #1*, that is the laminar inlet, and *Inlet #2,* the turbulent log profile. This comparison aims to display the self-similarity of the mean and turbulence statistics after canyon 3 or 4. Therefore, Fig. 3 confirms that by canyon #6 (the canyon that this paper will be focusing on) the flow characteristics are not as sensitive to the inflow conditions as they are from canyon #1 until canyon #3. This consideration is important given the variability of inflow conditions that can be present in urban environments. The results obtained following the present numerical setup are thus considered to provide a sufficient degree of comparability to general urban like inflow conditions over large neighbourhoods with similar geometries.

4 Validation

The code with the same numerical and domain setup was extensively validated in Llaguno-Munitxa et al. (2017). As such, here we will only provide a summary of these validations so the reader can appreciate the strengths and weaknesses of the LES for the flows investigated in this paper.

The numerical experiments (using Inlet #1) have been validated against the wind tunnel data collected by Llaguno-Munitxa et al. (2017) for canyon #6 and for three of the tested building geometries, the flat roof, pitched roof and round roof geometries. In figure (4), the LES mean and variance results are compared for canyon #6, and for the flat, pitched, and round roof geometries, against the wind tunnel results. The comparison of the wind tunnel and LES results for the flat roof geometry show a good agreement, with the largest discrepancies at heights between 1H and 2H for the mean velocities. The σ_t^2 (the sum of the streamwise and vertical variances that the hotwire captures) plots also display a good agreement with differences smaller than 15%. For the pitched roof geometry, the comparison of the mean velocity between the wind tunnel and LES results also shows a very good agreement with differences smaller than 5%; a similarly good agreement is observed for the case of the round roof geometry mean velocity. On the other hand, the σ^2 comparisons between the wind tunnel and LES results show larger discrepancies for both the pitched and round roof geometries in comparison to the σ^2 plots of the flat roofs or to the means. The wind tunnel and LES results agree qualitatively on higher turbulence levels for the pitched and round roofs in comparison to the flat roof; however, LES appears to overpredict the turbulence statistics in comparison to the wind tunnel results, especially so for the round roof geometry. Differences in the inlet velocity or an underestimation by the hot wire of the variance induced by the low velocity in the canyon might be possible causes for this discrepancy; however, it would be expected that such a mismatch would also influence the results of the flat roof and the means. Thus, the more plausible cause is that the LES has more difficulty in capturing the turbulence inside the canopy over non-flat roofs, and subsequently the turbulence levels inside as well as outside the canopy layer are affected. This is related to the fact that, for LES, capturing the separation correctly, particularly over round roofs, is more challenging. Temmerman et al. (2003) provides an in-depth analysis of the challenges of LES to model the flow over a round hill. For the flat roof, the separation occurs at the corner of the building and thus is easy to capture (Aynsley, 1999). However, for the other roofs with more complex shapes, the geometries do not impose a clear separation point, and so the LES might have more difficulty matching it exactly especially in simulations like ours where LES relies on wall-modelling. Moreover, the separation will also be sensitive to the effective *Re* of the simulation.

The results obtained for the flat roof geometry (using Inlet #1) have also been validated against data from Brown et al (2000) who, for a similar setup with an array of 7 buildings, studied the air flow and turbulence statistics. These validations have been reported in Llaguno-Munitxa et al. (2017) and will not be reproduced here. Vertical profiles have been compared for canyon #2, canyon #6 (the canyon where the LES results have been displayed), and downstream. The mean velocity profiles were found in very good agreement with differences of about 5%. The turbulent kinetic energy results display larger discrepancies than the mean velocity results; however the differences remain acceptable. Overall, the profile trends are captured accurately and the quantitative errors remain moderate.

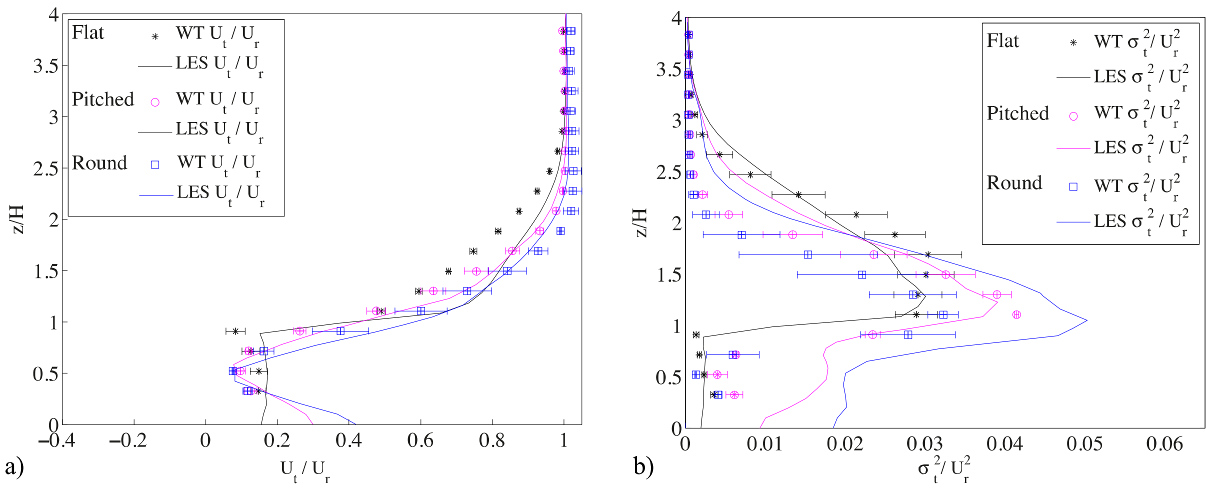

Fig 4 Wind Tunnel and LES result (with imposed Inlet #1 inflow conditions) comparison for canyon #6 until 4*H*. All values are normalized by the reference velocity U_r, which has been taken at 2.5*H* upstream. The left panel depicts the wind tunnel and LES wind speed, U_t, for the Flat roof, Pitched roof, and Round roof. U_t is the magnitude of the velocity vector, mainly composed of the streamwise and vertical components. The right panel depicts the corresponding wind tunnel and LES total variances σ_t^2. For more details refer to Llaguno-Munitxa et al. (2017).

5 Air Exchange Rate (ACH)

Air exchange from within a canyon generally can take place horizontally (along the street axis) and vertically (across the interface plane aligned with the roof vertices). For the archetypical urban street canyon studied in this paper however, the canyon is assumed to be very long such that the vertical exchanges are the principal source of clean fresh air. The studied building geometries therefore follow an idealized 2-dimensional 'infinite' building array configuration, and focus is therefore placed on the analyses of the vertical air exchanges. One must note however that real canyons can have complex 3-dimensional mean flow patterns where this assumption is not applicable.

The instantaneous vertical perturbation velocities w' have been saved from the LES runs for directly computing ACH at HP_1: the exchange at the plane of interface between the urban canopy layer and the free atmosphere, and HP_2: the exchange across a horizontal plane at the pedestrian level (see Fig. 5) for all studied building geometries. The instantaneous w' velocities for the vertical plane VP_1 as indicated in (Fig. 5) have also been saved to understand the variability of w' in the section plane. For all planes and sections, the same number and sequence of time-steps have been recorded and analyzed over about 120 eddy turnover times as detailed above.

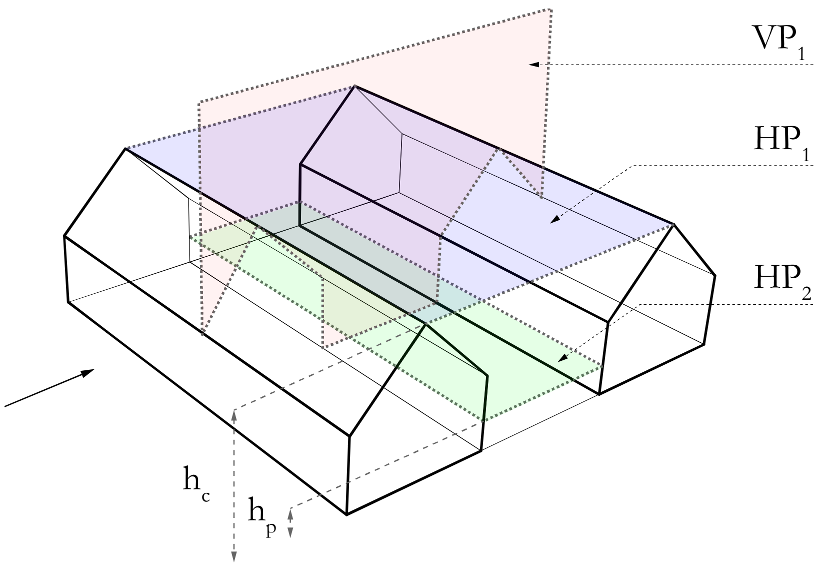

Fig 5 Air Exchange HP_1 and HP_2 and section plane VP_1 locations. The figure illustrates a limited section of the canyons; and VP_1 is in the middle of the domain span, halfway between the side walls.

5.1 *Direct LES ACH estimation*

The Air Exchange Rate calculations for the HP_1 and HP_2 planes have been performed by studying the flow across both planes for 20,000 time-steps (5s computed time) as described in section #3. The data have been saved at the cell centre for HP_1, HP_2, and VP_1. The number of cells in the studied HP_1 and HP_2 planes ranged from 1900 for the flat roof to 5520 for the pitched roof (bear in mind that the top exchange planes for the pitched and round roofs are twice larger and the terraced building exchange plane is 0.4H larger than the exchange plane for flat roof and geometry with balconies). For the VP_1 plane, the number of cells for the flat roof case was 800 and for the pitched roof it was 1111.

The vertical fluxes for HP_1 and HP_2 planes for a given street canyon volume are directly computed by integrating the mass flux out of the canyon following:

$$ACH_{LES}(m^3/s) = \underbrace{\iint_A \underbrace{\left(\frac{1}{T} \int_0^T w^+ \, dt \right)}_{\text{temporal averaging}} dA}_{\text{spatial integration}} \tag{6}$$

where T is the total time averaging period, that is, 5 s. A is the area of HP_1 or HP_2 planes over which the ACH has been computed. w^+ reflects the recorded instantaneous positive vertical velocities (while w^- that will be used later are the negative ones). This is essentially the time-average of the positive vertical velocity (flow exiting the canyon) at each point, integrated or summed spatially over the whole plane. Normalizing by the street canyon volume V_c (where the subscript c refers to the canyon, and h_c is the depth of the canyon) yields ACH* defined as:

$$ACH^*(s^{-1}) = \frac{ACH}{V_c} \tag{7}$$

From (Eq. 6) and (Eq. 7), for the simple case of a flat roof where $V_c = h_c A$, we obtain:

$$ACH^*(s^{-1}) = \frac{1}{h_c} \underbrace{\left(\frac{1}{A} \iint_A \underbrace{\left(\frac{1}{T} \int_0^T w^+ \, dt \right)}_{\text{temporal averaging}} dA \right)}_{\text{spatial averaging}} = \frac{1}{h_c} \langle \overline{w^+} \rangle . \tag{8}$$

The overbar here denotes temporal averaging, while the angled brackets denote spatial averaging. Distinguishing between these two averaging operators is very important in spatially-variable flows over complex terrain. For two-dimensional configurations with uniform street profiles in the longitudinal axis and with an invariant total air mass inside the canyon, continuity imposes that:

$$\left\langle \overline{w} \right\rangle = \left\langle \overline{w^{+}} \right\rangle + \left\langle \overline{w^{-}} \right\rangle = 0 \quad \Rightarrow \quad \left\langle \overline{|w|} \right\rangle = 2\left\langle \overline{w^{+}} \right\rangle. \tag{9}$$

Where the vertical bars denote the absolute value of w. Therefore, the ACH* can be estimated (again for the simple flat roof case for illustration) following:

$$ACH^{*}(s^{-1}) = \frac{ACH}{V_c} = \frac{1}{h_c}\left\langle \overline{w^{+}} \right\rangle = \frac{1}{h_c}\frac{1}{2}\left\langle \overline{|w|} \right\rangle. \tag{10}$$

If the roof is not flat, h_c in Eqs 8 and 10 should simply be replaced by an effective height $h_e = V_c/A$. As such, the exchanges are produced by (i) the turbulent perturbations from the temporal mean that modulate $\overline{w^{+}}$, as well as by (ii) the coherent patterns of the time-averaged mean flow that modulate $\left\langle \overline{w^{+}} \right\rangle$and produce the so-called dispersive fluxes. Note that if Eq. (9) does not hold and a mean flux $\left\langle \overline{w} \right\rangle \neq 0$ exists, Eq. (10) is still a correct expression that accounts for both turbulent and dispersive fluxes, but the mean flux needs to be added to get the total ACH. The dispersive and turbulent components are illustrated in figure 6 that depicts the flow field for the vertical plane VP_1. The pseudocolor plot shows the vertical turbulent rms velocity σ_w and the vector plot shows the mean (time-averaged) velocity patterns. As reported in the paper that precedes this research (Llaguno-Munitxa et al., 2017), σ_w substantially increases for the cases of the pitched and round roof geometries in comparison to the flat roof geometry. The round roof geometry is the case where the largest turbulence intensities are observed, regardless of what inflow is imposed. For the flat roof geometry, the stagnation point is located at the windward vertex of the roof corner, and for the pitched and round roofs it is located in the middle of the windward roof slopes. The flow separation point on the other hand, occurs at the leeward vertex for the flat roof, slightly below the crest for the pitched roof, and almost half way down the leeward roof side for the round geometry. In all cases, the highest turbulence levels are observed in the shear zone near the roof level, but the depth of this zone varies for the different cases. For the pitched and round roofs, the roof shape creates a strong downdraft inducing higher turbulent intensities and mean flow. The roof set-back produces a similar, but less intense, effect. Balconies, on the contrary, limit the flow access to the canyon, reducing the air circulation entrance in the windward face and consequently reducing σ_w over and below the shear layer.

Within the canyon, the round roof geometry generates the largest $\sigma_{w,}$ while the flat roof reduces the vertical turbulent exchanges between the urban canopy layer and the free atmosphere. The terraced building, in comparison to the flat roof, increases the mean and turbulence velocities within canyon; however, the effect of terraces appears to be subtle in comparison to the changes produced by the other geometries. In all cases, a flow recirculation is discernible within the street canyon. It is also observable that the presence of balconies promotes the stagnation of air within the canyon, reducing the strength of the standing vortex as well as the turbulence intensity. In a similar way, the balconies seem to be interfering with the smaller eddies substantially reducing σ_w within the canyon.

Many of the qualitative results observed for the VP_1 plots are also observable in Fig .7 that depicts *ACH* sections. Horizontal transects along the central *x*-axis of the ACH planes have been gathered to compare $\overline{w}$ and σ_w profiles for the studied building geometries. Figure (7a) displays a comparison of the $\overline{w}$ plots for HP_1 (note that the width of the exchange plane is variable for the different geometries). The pitched and rounds roofs show the largest $\overline{w}$ velocities, especially in the ACH area adjacent to the downstream roof slope. This implies that they generate the largest dispersive fluxes. In both cases (and especially for the case of the pitched roof geometry), the flow separation as observed in Fig. 6, creates a strong downdraft which explains the increase in the negative $\overline{w}$ and associated increase in the positive one further downstream. A similar effect is observed for the set back roof, but to a reduced extent. The flat roof and the building with balconies show similar tendencies. The differences observed between the studied geometries are most visible for the σ_w plots in (Fig. 7b). The round roof shows the largest turbulence levels in the HP_1 plane followed by the pitched roof. Similarly to the $\overline{w}$ plot, particularly for the case of the round roof geometry, the largest σ_w are observed adjacent to the downstream roof slope. The set back roof shows similar tendencies, but the turbulent intensities are smaller than for the pitched and round roof geometries. The flat roof and building with balconies geometries are the ones with lowest σ_w.

While *ACH* is generally computed in planes analogous to HP_1 where the exchanges are generally largest given the proximity of the plane to the shear layer, it is most likely that *ACH* planes that are closer to the ground level or pedestrians, such as HP_2, will be the locations in the Urban Canopy Layer (UCL) where the lowest turbulence intensity and vertical velocities occur. Therefore, given the importance of the lowest layer of the canyon for pedestrian exposure to pollution and heat, this area is probably more critical in terms of urban ventilation that the whole canyon ventilation assessed at HP_1. The two should be analyzed together to ensure that fresh air not only makes it into the canyon (through HP_1), but also to pedestrian level (through HP_2). Fig. 7c shows $\overline{w}$ for HP_2. The within canyon vortex is most visible for the case of the round roof where a larger velocity gradient is observed between the upstream and downstream faces. The pitched and flat roof geometries display very similar $\overline{w}$ magnitudes. The balconies and set back roof geometry, show the lowest $\overline{w}$ velocities, denoting a weaker within canyon vortex. Fig. 7d shows the σ_w plots for HP_2. The results show similar trends to those observed in Fig. 7b for HP_1. The HP_2 of the round roof geometry displays the highest σ_w, followed by the pitched roof and the set back and flat roof geometries. The geometry that generates the lowest σ_w at the HP_2 plane is the geometry with the façade with balconies, as was the case at HP_1. In general, for both planes, the geometries that produce the strongest dispersive exchanges also produce the strongest turbulent exchanges.

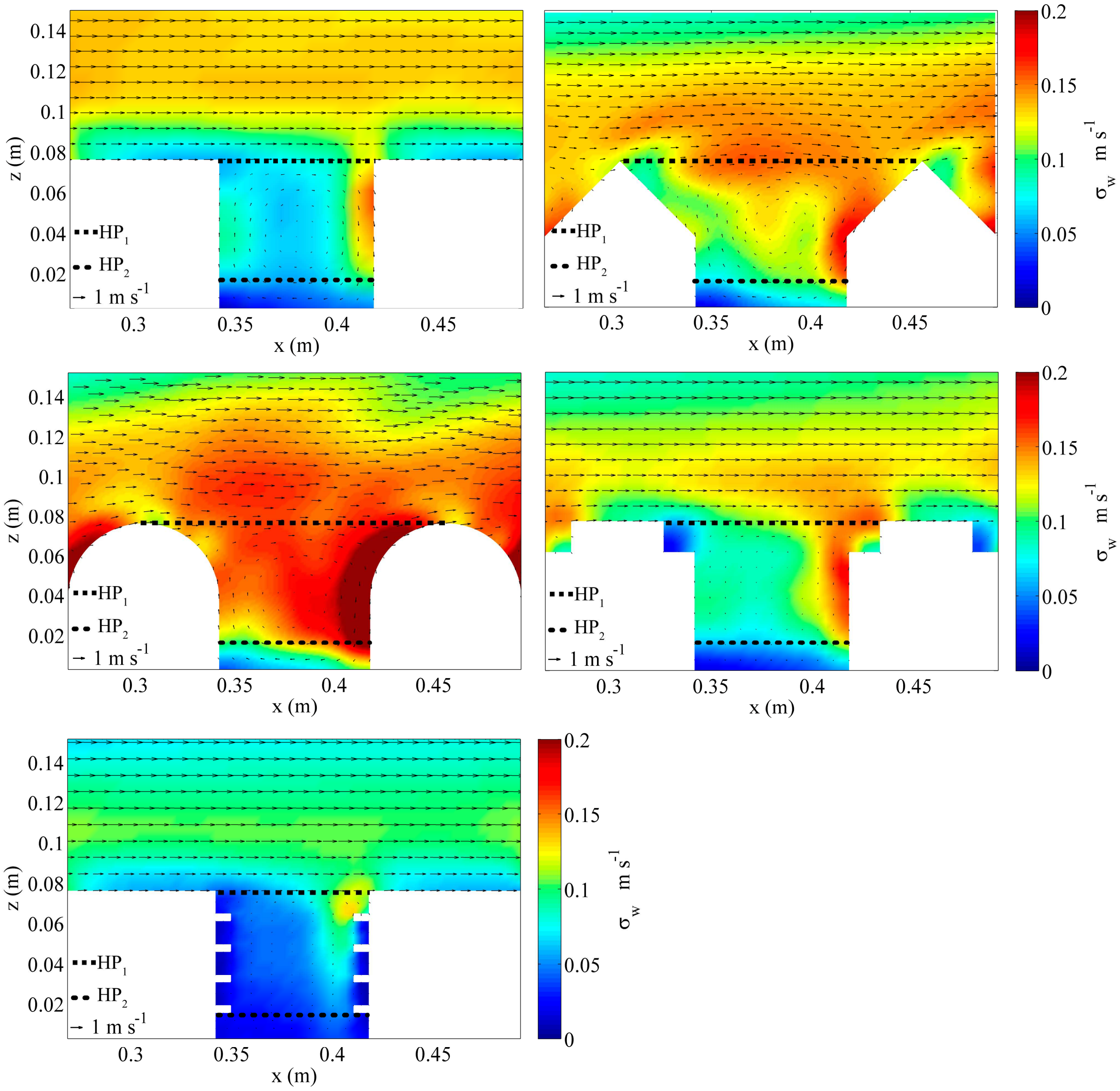

Fig 6 LES results for air flow and vertical turbulence intensity for the 5 different building geometries. The time-averaged velocity is displayed with the vector plot, and σ_w with pseudocolor plots. The thick dashed lines denote the locations of the exchange planes considered.

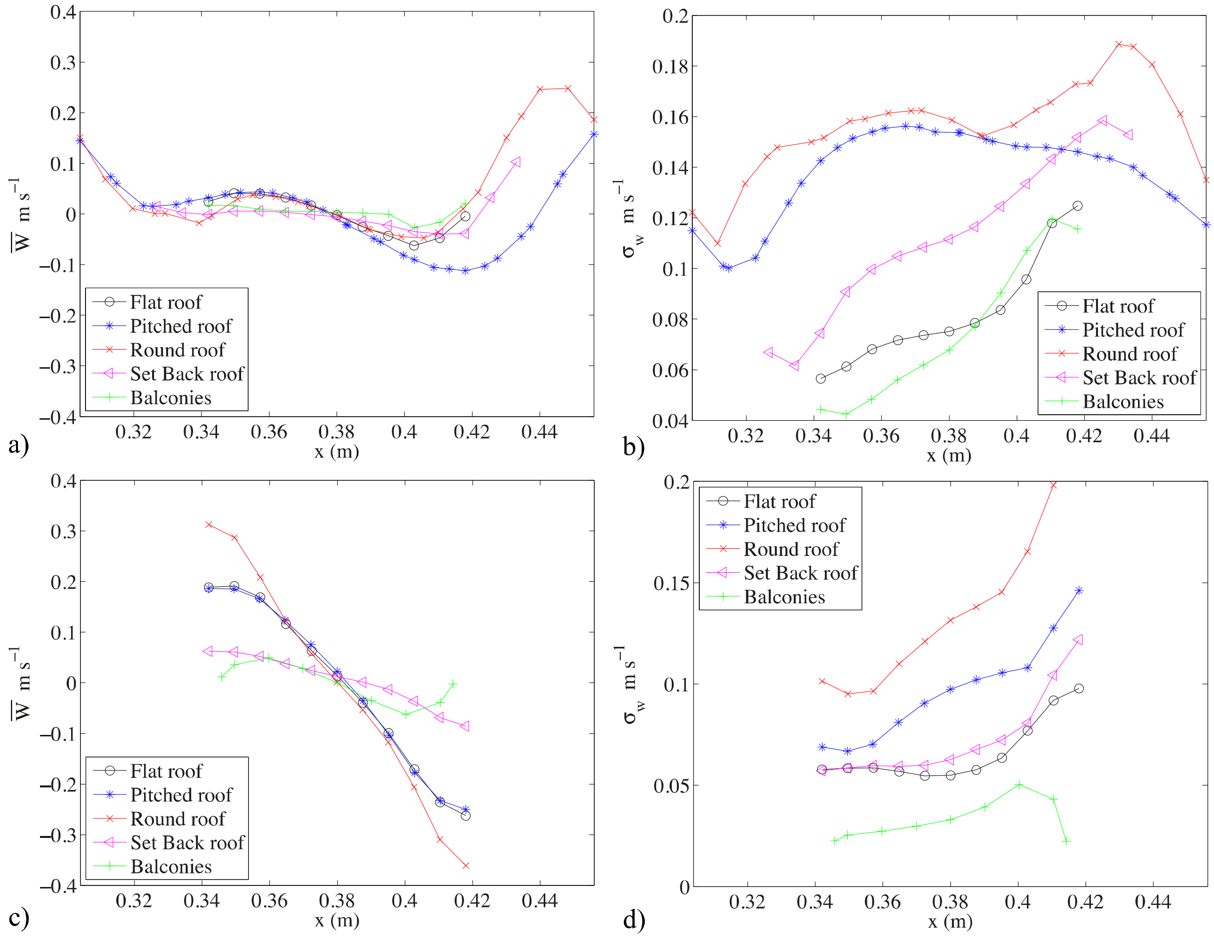

Fig 7 LES results for spatially-averaged (along the street canyon longitudinal axis, *y*-direction) exchange planes HP_1 and HP_2: a) the mean vertical velocity $\overline{w}$ for HP_1; b) σ_w for HP_1; c) the mean vertical velocity $\overline{w}$ for HP_2; and d) σ_w for HP_2. Note that the rakes displayed in the figure, show the data computed for the ACH planes HP_1 and HP_2, which only cover the central area of the canyon, thus the portions adjacent to the walls have not been included (which explains why the mean velocity averages over *x* would not be exactly 0 for all cases).

The formulation described in Eq. (10) has been followed to calculate the direct LES estimation ACH^*_{LES} (including turbulent and dispersive exchanges) for the HP_1 and HP_2 planes. Table (2) shows the results for plane HP_1 and Table. (3) shows the results for plane HP_2. These two tables also show the extrapolation of the obtained results to *real* building prototype scales. For scaling to the real world from the LES results, the non-dimensional parameter that can be considered invariant to scale (if the *Re* sensitivity effects are ignored) is the exchange velocity to reference velocity ratio U_e/U_{ref}. This ratio is hence the same for the LES model and real world prototype. Since ACH = $U_e\,A_c$, one can then write

$$ACH^{real} = U_e^{real} A^{real} = \frac{U_e^{real}}{U_e^{LES}} U_e^{LES} \frac{A^{real}}{A^{LES}} A^{LES} = \frac{U_e^{real}}{U_e^{LES}} \frac{A^{real}}{A^{LES}} ACH^{LES}. \quad (11)$$

In agreement with the patterns observed in Fig. 5 and Fig. 6, the round roofs show the largest ACH^*_{LES}, followed by the pitched roof, the set-back geometry, the flat roof, and the geometry with balconies, with results over four times smaller for the geometry with balconies in comparison to the round roof geometry at HP_1, and over 5 times smaller at HP_2. The equivalent real building was assumed to have $U_{ref} = 2\ ms^{-1}$ and $H = W = 15m$ for the following calculations (following a 1/200 scale ratio between the LES and real prototype). In LES the longitudinal length of the exchange planes is 0.68 m (note that the HP_1 and HP_2 exchange planes do not extend to the lateral walls) and its equivalent real prototype length (following the same 1/200) results in 137m. The ACH_{Real} is then computed from Eq. (11) with $U_e^{real} / U_e^{LES} = 2/1.8$ and $A^{real} / A^{LES} = 200^2$.

Table 2 HP_1 LES and real prototype scaled based on Eq. 11.

Building Geometries	ACH^*_{LES} (s^{-1})	A_c (m^2)	V_c (m^3)	$ACH_{LES} = V_c\, ACH^*_{LES}$ ($m^3\, s^{-1}$)	ACH_{Real} ($m^3\, s^{-1}$)
Flat Roof	0.3973	0.0519	0.00395	0.00156	69.332
Pitched Roof	1.0619	0.1039	0.00493	0.00524	232.886
Round Roof	1.6504	0.1039	0.00437	0.00721	320.441
Façade Set-back	0.6096	0.0727	0.00426	0.00259	115.109
Façade Balconies	0.3333	0.0519	0.00395	0.00131	58.221

Table 3 HP_2 LES and real prototype scaled based on Eq. 11.

Building Geometries	ACH^*_{LES} (s^{-1})	A_c (m^2)	V_p (m^3)	$ACH_{LES} = V_p\, ACH^*_{LES}$ ($m^3\, s^{-1}$)	ACH_{Real} ($m^3\, s^{-1}$)
Flat Roof	1.3657	0.0519	0.00197	0.00268	119.109
Pitched Roof	2.1067	0.0519	0.00197	0.00415	184.442
Round Roof	2.1747	0.0519	0.00197	0.00428	190.220
Façade Set-back	0.7945	0.0519	0.00197	0.00156	69.332
Façade Balconies	0.4357	0.0519	0.00197	0.00085	37.777

5.2 *ACH^* estimation from RANS*

As addressed by Cheng et al. (2009) and Li et al. (2005), the difference between the computation time of RANS and LES models is very large. Urban planning and architectural design processes require fast decision-making and therefore the time and expertise required to perform LES calculations are generally not available. Therefore, it is worth looking into alternative estimates of ACH that require less computationally demanding simulations such as RANS.

With this ambition, Li et al. (2005) described a formulation as an alternative to their previously published LES based ACH computation (Liu et al., 2005). Their formulation based on the results obtained from a RANS *k-ε* model related the ACH to the perturbation velocity at the exchange plan of interest following:

$$ACH_{\sigma w} = \frac{1}{2}\iint_A \overline{w'w'}^{1/2}\, dA = \frac{1}{2} A\langle \sigma_w \rangle, \tag{12}$$

where the primes denote the perturbation velocity relative to its ensemble mean, which could be surrogated by the time average (but not the spatial average). This formulation makes some simplifications that we will revisit later in the paper. Furthermore, isotropic turbulence was assumed in the street canyon in previous studies to relate the standard deviation of vertical velocity to the turbulent kinetic energy (k) that is available from RANS with a closure such as k-ε:

$$k = \frac{\left(\overline{u'u'} + \overline{v'v'} + \overline{w'w'}\right)}{2} \approx \frac{3\overline{w'w'}}{2} \quad \Rightarrow \quad \sigma_w = \overline{w'w'}^{1/2} \approx \left(\frac{2}{3}k\right)^{1/2}. \tag{13}$$

By combining (eq. 12) and (eq. 13), this ACH estimate leads to the following equation:

$$ACH_{\sigma w} = \frac{1}{\sqrt{6}}\iint_A \sqrt{k}\, dA = \frac{1}{\sqrt{6}} A\langle \sqrt{k} \rangle. \tag{14}$$

However, as observed in Figs. 6 and 7, $\overline{w}$, $\overline{u}$, σ_w and σ_u are substantially different for the various geometries. Therefore, assuming that the turbulence is isotropic might not be an adequate simplification. For such assumption to be more accurate, a degree of isotropy should be defined for the different building geometries as well as for the different *ACH* planes. Perhaps the more important point to underline is that the estimation proposed by (Li et al., 2005) does not take into account the mean and dispersive fluxes. In spatially-variable flows such as the one we study here, even if the spatially and temporally averaged (mean) velocity at the plane of interface is zero, the spatial variability of the time-averaged velocity field results in a dispersive flux (Poggi and Katul, 2008; Raupach and Shaw, 1982), as we noted earlier. Moreover, in realistic 3D canopies, even the spatially and temporally averaged mean vertical velocity might not be zero. Another approach for ACH estimation proposed by Cheng et al. (2008) followed the formulation of Li et al. (2005) and proposed an alternative based on the eddy covariance method; it confirmed the point we underline here that the mean dispersive component was important and therefore has to be considered.

Moonen et al. (2011) proposed an alternative formulation for RANS simulations when the turbulence statistics are not known; this *ACH* estimation is based on the vertical velocity component:

$$ACH_w = \iint_A \frac{\overline{w} + |\overline{w}|}{2} dA, \tag{15}$$

This formulation also only requires RANS. It accounts for the mean fluxes (via the spatial integration of $\overline{w}$) and the dispersive fluxes (via the spatial integration of the absolute value of the time averaged velocity $|\overline{w}|$), but it ignores the turbulent fluxes. The authors indeed conclude that the impact of the turbulent contribution is significant and should be accounted for.

In tables 4 and 5 the results obtained following a σ_w-based $ACH^*_{\sigma w}$ estimation as given in Eq. (12) following Cheng et al. (2008), Li et al. (2005) and a time-averaged vertical velocity $\overline{w}$ based formulation ACH^*_w following Eq. (15) by Moonen et al. (2011) are provided. ACH^*_w significantly underestimates the *ACH* specially for the top plane compared to the LES direct calculations. This is despite the fact that ACH^*_w includes the (mostly positive but small) mean exchanges that are non-zero as shown in the tables and that are excluded from the ACH_{LES} based on Eq. (10) (the small mean flux is due to the fact that we exclude the regions adjacent to the sidewalls and thus the flow is not perfectly homogeneous in the cross-stream direction). $ACH^*_{\sigma w}$ performs well for the top plane (where the time averaged velocities are small as shown in Fig. 7), but large errors occur for HP_2 where the contribution of the dispersive transport is more significant due to larger $\left|\overline{w}\right|$. The estimate that assumes isotropy to infer σ_w based on k (eq. 14) is not included, but it will necessarily be inferior to the ones based directly on σ_w since it involves further simplifications.

Since these two formulations are both not satisfactory, we propose here a new formulation based on the folded normal distribution as an alternative for estimating the *ACH* from RANS. This formulation uses the mean vertical velocities $\langle \overline{w} \rangle$ and vertical turbulence statistics σ_w, which can be obtained through CFD simulations based on RANS with closures that provide this variance (e.g. second-order closures), or alternatively by assuming isotropy if only k is available such as in models with a k-ε closure (these are the most common codes in practice).

Fluent provides us with the time averaged $\overline{w}$ and σ_w ; recall that the time averaged velocity $\overline{w}$ at a given location is not zero. Therefore, at every point in space we can define $w = \overline{w} + w'$. Two challenges arise when trying to compute the ACH. The first is that summation and taking the absolute value are not commutative operations and therefore, referring to Eq. (10), $\overline{|w|} = \overline{|\overline{w} + w'|} \neq \overline{|\overline{w}| + |w'|} = \overline{|\overline{w}|} + \overline{|w'|}$ and by extension $|\overline{w'}| \neq \overline{|w'|}$ (note however that for the mean we can write $\overline{|\overline{w}|} = |\overline{\overline{w}}| = |\overline{w}|$). The second challenge arises since time averaging and squaring are also not commutative operations and hence the variance σ^2_w, which can be computed directly from LES or from RANS (assuming isotropy if needed), cannot be used to inform us on $\overline{|w'|}$ since $\sigma_w^2 = \overline{w'^2} = \overline{|w'^2|} = \overline{|w'|^2} \neq \overline{|w'|}^2$ (note that this inequality is ignored in the model of Li et al. (2005) presented in Eq. (12), resulting in the cancellation of the dispersive flux contributions). These challenges imply that the actual exchange, which is related to $\overline{|w|}$ cannot, in general, be exactly related to the mean and the standard deviation of w.

To overcome this hurdle, we will assume that w has a normal (Gaussian) distribution. Figure 8 shows the probability distributions of w' for all studied building geometries and the two studied exchange planes HP_1 and HP_2, and compares them to the Gaussian distribution curve. The plots show that the distribution of w' for all different building geometries is very well approximated by the Gaussian. There are discrepancies at the tails but these tails are very infrequent (notice the log-scale of the y axis) Therefore, this implies that $|w|$ can be assumed a folded normal distribution (Leone et al., 1961) and its mean (time average) $\overline{|w|}$ can be related to $\overline{w}$ and σ_w at each spatial point, and then averaged in space to get the ACH following Eq. (10). The folded normal distribution of a Gaussian variable w is the distribution of its absolute value $|w|$, which will have the following mean:

$$\overline{|w|} = \sqrt{\frac{2}{\pi}}\sigma_w \exp\left(-\frac{\overline{w}^2}{2\sigma_w^2}\right) - \overline{w}\, erf\left(-\frac{\overline{w}}{\sqrt{2}\sigma_w}\right), \quad (16)$$

where *erf* is the error function. Therefore the ACH equation (following from Eq. (10) becomes:

$$ACH_{FND} = \frac{A_c}{2}\left\langle \sqrt{\frac{2}{\pi}}\sigma_w \exp\left(-\frac{\overline{w}^2}{2\sigma_w^2}\right) - \overline{w}\, erf\left(-\frac{\overline{w}}{\sqrt{2}\sigma_w}\right)\right\rangle. \quad (17)$$

In Tables 4 & 5, a comparison of the ACH calculation methodologies ACH^*_{LES}, ACH^*_{FND}, $ACH^*_{\sigma w}$, and ACH^*_{w} are included in columns 1, 2, 3, and 4, respectively, for the different building geometries. Note that the * here denotes that the provided ACH_{LES}, ACH_{FND}, $ACH_{\sigma w}$ and ACH_w results have been normalized based on their respective canyon volumes, V_c and V_p reported in tables 2 and 3, for the top and bottom exchange planes HP_1 and HP_2, respectively. The mean $\langle \overline{w} \rangle$, dispersive $\langle \overline{|w|} \rangle$, and the turbulent σ_w exchange velocity have also been included in columns 5, 6 and 7 respectively. It is important to remember that the formulations for ACH^*_{LES} and ACH^*_{FND} include the combined effect of the dispersive and the turbulent fluxes, while $ACH^*_{\sigma w}$ only accounts for the turbulent fluxes and ACH^*_{w} only takes into account the mean and dispersive fluxes (these formulations can be directly recovered from the corresponding exchange velocities upon dividing by $2 \times h_c$ (recall h_c is the effective canyon depth)).

For the case of HP_1, as shown in in Column 3 of Table 4, the ACH^*_{FND} model is the one that produces the closest results to ACH^*_{LES}, with deviations below 2%. The second best performing model for HP_1 is $ACH^*_{\sigma w}$. This is not surprising given that at the interface of the urban canopy layer is where the highest turbulent fluxes are observed. Thus for HP_1, larger discrepancies are observed between ACH^*_{w} and ACH^*_{LES}.

In Column 2 of Table 5, the folded estimate ACH^*_{FND} is shown for HP_2. As for HP_1, the results obtained following the folded estimate show a very good agreement with deviations smaller than 2%. As for HP_1, the round roof geometry shows the largest direct LES estimate followed by the pitched roof, the set-back geometry, the flat roof, and the geometry with balconies. The exchanges are 5 times larger for the round geometry than for the geometry with balconies. But for the case of HP_2, the contribution of $\langle \overline{w} \rangle$ and σ_w becomes more geometry dependent, thus the $ACH^*_{\sigma w}$ results show larger disagreements with ACH^*_{LES} results than those observed for HP_1. ACH^*_w on the other hand shows closer results to ACH^*_{LES}, given that at HP_2 the dispersive fluxes are more dominant (compare the corresponding exchange velocities at the two planes).

Overall, the results obtained following the folded estimate method ACH^*_{FND} show excellent agreement with the direct LES estimates. Thus based on the studies included in this paper, the model ACH^*_{FND} produces the estimates that best match the results obtained through the direct LES computations, revealing the importance to account for both the dispersive and turbulence fluxes in the *ACH* estimation methodologies. The skill of the *FND* method is not surprising since, following Eq. (17), the results obtained by ACH^*_{FND} should exactly match the ACH^*_{LES} if the obtained velocity measurements where exactly Gaussian. Since figure 8 illustrates, the deviation from the Gaussian is only observed at the tails of the plot (again note the log-scale of the *y* axis). At the peaks that are more frequent, the results display a Gaussian distribution, resulting in the good match between the ACH^*_{LES} and ACH^*_{FND}.

The exchange velocities listed in Tables 4 and 5 further illustrate that both turbulent and dispersive fluxes are important, though turbulent exchanges dominate near the canyon top, while dispersive ones dominate near street level. The mean fluxes in our 2-dimensional configuration are negligible, but again not exactly zero since the configuration is not truly infinite and homogeneous in the cross-stream direction and since we exclude regions near the walls.

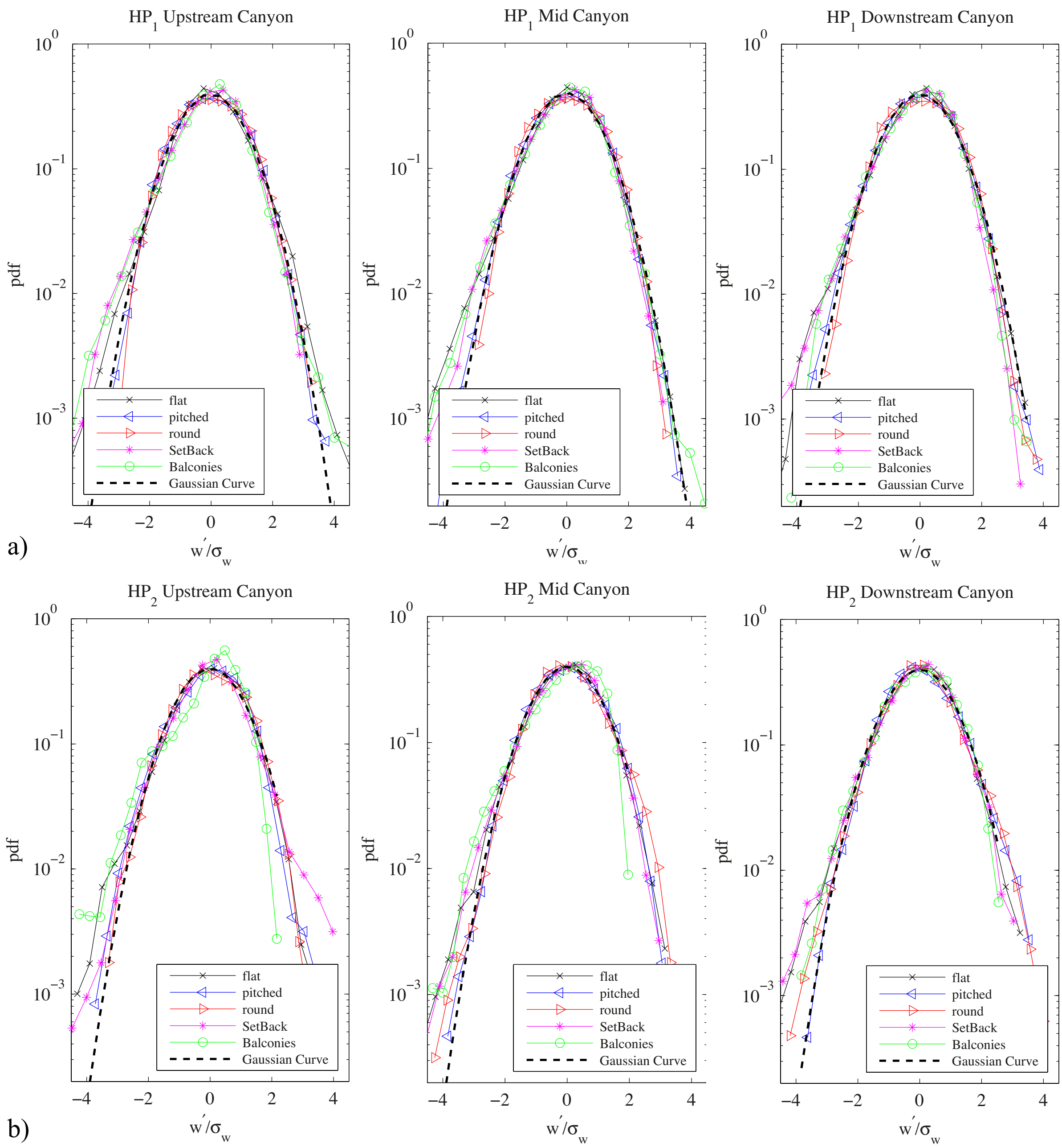

Fig 8 Probability distributions for the perturbation velocity *w′* for cross-stream lines at various streamwise locations for all studied building geometries. Upper panel a) shows the results obtained for the top plane HP_1. The figure to the left shows the mid canyon (in the *x*-direction) distribution plot followed by the leeward (upstream when looking at a canyon, middle panel) and downstream (downstream when looking at a canyon, right panel) canyon facades. Lower panel b) shows the results obtained for the bottom plane HP_2. The figure to the left shows the mid canyon plot, again followed by the leeward and windward distributions. All results can be reasonably approximated by the Gaussian distribution depicted by the dashed black line, despite discrepancies at the tails that are significant for exchanges.

Table 4 *HP_1* air exchange rates

Building Geometries	ACH^*_{LES} (s^{-1})	ACH^*_{FND} (s^{-1})	$ACH^*_{\sigma w}$ (s^{-1})	ACH^*_{w} (s^{-1})	$\langle \overline{w} \rangle$ ($m \times s^{-1}$) *(mean exchange velocity)*	$\langle \lvert \overline{w} \rvert \rangle$ ($m \times s^{-1}$) *(dispersive exchange velocity)*	σ_w ($m \times s^{-1}$) *(turbulent exchange velocity)*
Flat roof	0.3973	0.4006	0.3113	0.4044	0.0134	0.0481	0.0474
Pitched roof	1.0619	1.0609	1.1273	0.5249	–0.0004	0.0502	0.1070
Round roof	1.6504	1.6311	1.5655	1.2175	0.0277	0.0747	0.1317
Set back roof	0.6096	0.6141	0.7196	0.2867	0.0075	0.0261	0.0843
Façade balconies	0.3333	0.3303	0.3635	0.2312	0.0146	0.0206	0.0553

Table 5 *HP_2* air exchange rates

Building Geometries	ACH^*_{LES} (s^{-1})	ACH^*_{FND} (s^{-1})	$ACH^*_{\sigma w}$ (s^{-1})	ACH^*_{w} (s^{-1})	$\langle \overline{w} \rangle$ ($m \times s^{-1}$) *(mean exchange velocity)*	$\langle \lvert \overline{w} \rvert \rangle$ ($m \times s^{-1}$) *(dispersive exchange velocity)*	σ_w ($m \times s^{-1}$) *(turbulent exchange velocity)*
Flat roof	1.3657	1.3668	0.5642	1.3739	0.0055	0.0988	0.0428
Pitched roof	2.1067	2.1070	1.2169	2.0064	0.0090	0.1434	0.0924
Round roof	2.1747	2.1792	1.3311	1.9795	0.0052	0.1451	0.1011
Set back roof	0.7945	0.8087	0.6443	0.6933	0.0044	0.0482	0.0489
Façade balconies	0.4357	0.4390	0.2790	0.3659	-0.0011	0.0289	0.0212

5.3 Pollutant Concentration (PC) estimation

To infer pollutant concentration from LES or RANS for a given case, the most direct and accurate way is to solve the budget equation of a tracer (that could be reactive). If one then aims to estimate pollutant concentration at pedestrian level, the influence of geometry, as well as location of the pollutant emission and reactivity of that chemical, can be captured. Since pollutant emissions and transport were not directly simulated in our LES, a pollutant concentration estimation formulation is proposed to compare the impacts on the pollutant concentration levels of the studied building geometries. This method is not as accurate as the direct simulation of a tracer, but it has the advantages of (i) not focusing on a specific pollutant emission location, and (ii) being applicable to wind tunnel data (where a pollutant concentration is difficult to measure) or other CFD results that cannot capture tracer budgets (either existing data or for codes where passive tracers are not included). As such, it is generally useful to be able to estimate, albeit approximately, pollutant concentrations and how they are influenced by geometry from air exchange considerations alone.

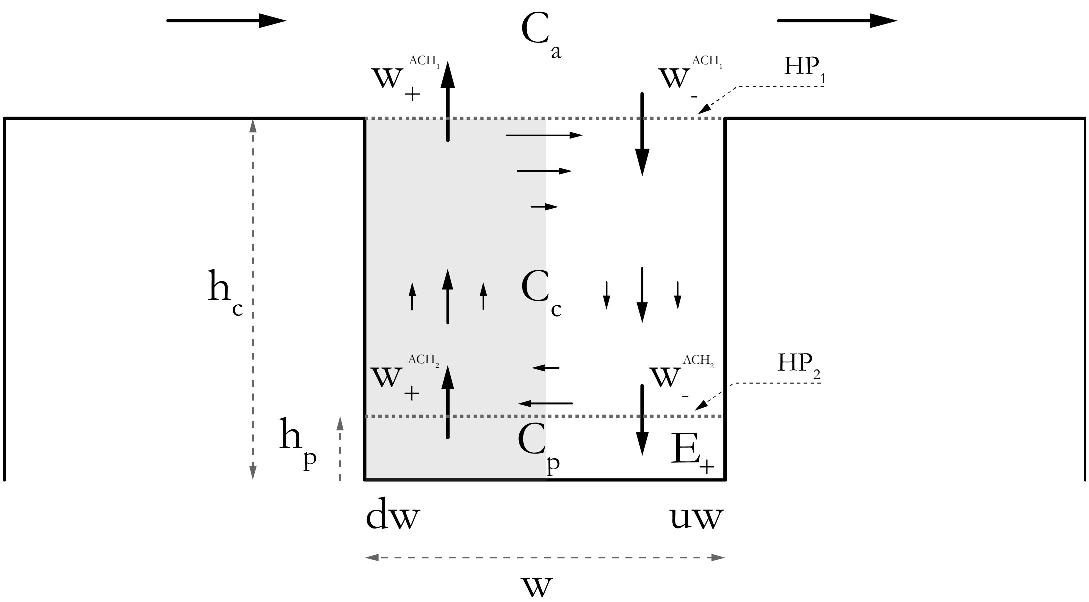

Fig 9 Street canyon pollutant exchange diagram.

The pollutant exchange between the canyon and the free atmosphere, that is through plane HP_1 is determined by the vertical exchanges w^+ and w^- as depicted in (Fig. 9). C_a is the free atmosphere concentration. If the canyon is assumed to consist of one well-mixed reservoir, C_c would be the average canyon concentration below HP_1 in this one-reservoir model. A_C refers to the area of the HP_1 plane. E_+ stands for the pollutant source emission rate (in kg s^{-1}).

Therefore, the variability in the concentration C_c will depend on the time t it takes to exchange the volume of air contained within the canyon. Using a simple mass balance model that assumes that air leaving the canyon is at C_c and air entering is at C_a (we will revisit this assumption later):

$$V_c \frac{dC_c}{dt} = \left(-\left\langle \overline{w^+} \right\rangle C_c + \left\langle \overline{-w^-} \right\rangle C_a \right) A_c + E. \qquad (18)$$

All terms have dimensions of mass over time. As described in the prior section, we can replace w^+ and $-w^-$ with the absolute mean velocity statistics $\langle|\overline{w}|\rangle/2$:

$$V_c\frac{dC_c}{dt}=\frac{\langle|\overline{w}|\rangle}{2}\left(-C_c+C_a\right)A_c+E. \tag{19}$$

Under steady state, this yields:

$$C_c-C_a=\frac{2}{\langle|\overline{w}|\rangle}\times\frac{E}{A_c}. \tag{20}$$

Using eq. (10) we can then write

$$C_c-C_a=PC=\frac{E}{ACH^{*}\,h_c\,A_c}=\frac{E}{ACH}. \tag{21}$$

Following Eq. (21), and knowing the pollutant emission rates and the computed ACH as per (Eq. 10), the concentration within the street canyon can be estimated. CO is used here as an example, and an estimation of the emission rate is performed following the guidance of (EPA, 2008, 2014) where the average gasoline vehicle emission rate is estimated to be 5.8 g CO km^{-1} (for an approximate velocity of 30 km h^{-1}). From this reference, we obtain that each vehicle emits 0.048 g CO s^{-1}. A density of about 145 vehicles per km of road (Ingram and Liu, 1999; NYSDOT, 2011) is assumed; therefore, for a road section with a length of 0.137 km, the emission of 19 cars has been presumed, which would yield a CO emission rate of 912 mg CO s^{-1}.

According to the EPA National record on CO Air Quality trends, a reasonable estimate for the average CO concentration in the atmosphere C_a is 3 mg CO m^{-3}. Based on the ACH estimations obtained for the real scale buildings (as shown in Table. 2 & 3) and following the emission rate of 912 mg CO s^{-1}, and the above described concentration in the atmosphere C_a, the pollutant concentration estimations can be computed. However, since the concentration at ground level, i.e. below HP_2, can be significantly higher than the canyon-average, this approach can be extended to a two-reservoir model to estimate the pollutant concentration to which pedestrians are exposed.

Assuming that the emissions are released below HP_2, they first have to get to the upper part of the canyon through HP_2, and then leave the canyon through HP_1. We can then write under steady state

$$\left(\eta_p C_p - C_c\right) ACH_2 = E, \tag{22}$$

where C_p is concentration at pedestrian level, C_c is concentration between planes HP_1 and HP_2 . η_p is the ventilation efficiency at the pedestrian introduced to account for the fact that the air below and above HP_2 are not truly perfectly mixed. Polluted air lofted upwards in the canyon might be re-entrained down below HP_2. This then yields:

$$C_c = \eta_p C_p - \frac{E}{ACH_2}, \tag{23}$$

The mass balance for the air space between HP_1 and HP_2, under steady state, then reflects the fact that pollutant flux through HP_1 and HP_2 must be equal, which when combined with Eq 23 yields

$$\begin{aligned} E &= \left(\eta_p C_p - C_c\right) ACH_2 = \left(\eta_c C_c - C_a\right) ACH_1 \\ &= \left(\eta_c \left(\eta_p C_p - \frac{E}{ACH_2}\right) - C_a\right) ACH_1 = \left(\left(\eta_c \eta_p C_p - C_a\right) ACH_1 - \frac{\eta_c ACH_1 E}{ACH_2}\right) \end{aligned} \tag{24}$$

Where η_c is the ventilation efficiency at the street canyon top, again introduced to account for re-entrainment of polluted air into the canyon. From this formulation, we can therefore obtain the value for C_p as a function of E

$$C_p = \frac{C_a}{\eta_c \eta_p} + \left(\frac{1}{\eta_c \eta_p ACH_1} + \frac{1}{\eta_p ACH_2}\right) E \tag{25}$$

HP_1 and HP_2, thus act like resistances in series to the ventilation of pollutant from the street level. One should note here that the ventilation efficiencies can only be exactly estimated from simulations where the pollutant is actively represented as a tracer. Their values will depend on many factors such as emitter locations and geometry. As such, the influence of geometry can exceed what is inferred from differences in ACH if it turns out it has a big impact on ventilation efficiency. This however would require another study that delves into such analyses and cannot be adequately addressed in this paper. Therefore, here we will restrict the scope to investigating the influence of variations in the values of η_c and η_p on the concentrations.

This concentration, denoted as C_p (following Eq. 25), accounts for the concentration of air contained below HP_2, while C_c in this two-reservoir model (following Eq. 23) denotes the pollutant concentration contained between HP_1 and HP_2 (see Fig. 9). The emitter has been assumed to be located fully below HP_2, representing the CO emissions released from the circulating passenger vehicles.

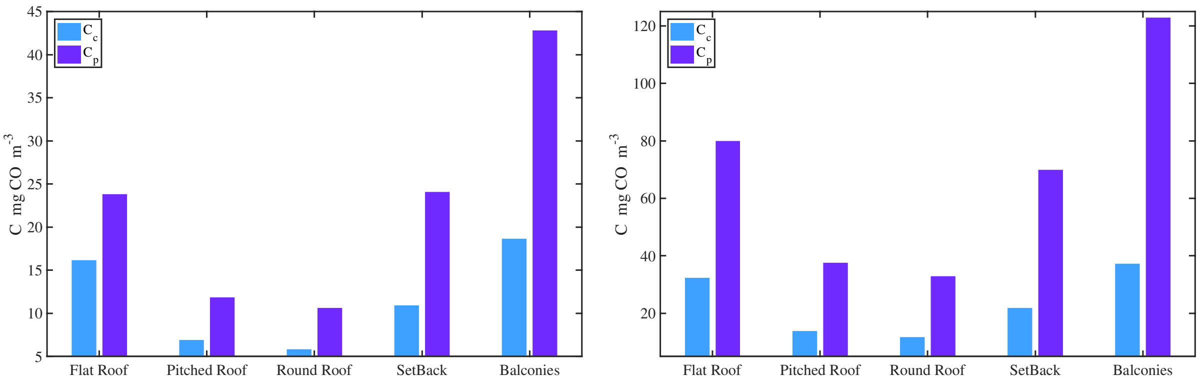

a) b)

Fig 10 Street canyon pollutant exchange: the blue colour bars display the C_c results (the *PC* contained between HP_1 and HP_2) while the purple colour displays the C_p results (the *PC* contained below HP_2) a) shows the results obtained for a ventilation efficiency of $\eta_p = \eta_c = 1$, while b) shows the results obtained for a ventilation efficiency of $\eta_p = \eta_c = 0.5$.

Figure (10) displays the concentrations computed following Eqs. (23) and (25). Two cases have been studied (i) with a ventilation efficiency of $\eta_p = \eta_c = 1$ (an overly optimistic scenario where the full volume of air within the canyon would be exchanged in one event), and (ii) with a ventilation efficiency of $\eta_p = \eta_c = 0.5$ (where exchanges occur in smaller volumes allowing some emitted pollutants to remain in the canyon following the exchange of a full volume; this results from the effect of re-entrainment for example and the shortcomings of the fully-mixed reservoir assumption. Taking into account that the current NAAQS for CO establish an environmental limit of 9 mg m^{-3} of carbon monoxide (EPA, 2010), the computed concentrations included in (Fig. 10a) following $\eta_p = \eta_c = 1$ remain within tolerable limits for the pitched and round roof geometries; however, the remaining geometries exceed the EPA limit. Figure 10.b, where $\eta_p = \eta_c = 0.5$ is used, shows that the pollutant concentrations both for C_p and C_c exceed the tolerable limits for all studied building geometries. This in fact underlines the limitations of air exchange studies if not coupled with analyses of ventilation efficiency. As shown in (Fig. 10.b), C_p ranges from 32.97 mg m^{-3} (for the round roof building geometry) to 122.94 mg m^{-3} (for the building geometry with balconies). Overall it is clear that, as discussed for the *ACH* results, the pollutant concentrations both at the pedestrian level and across HP_2 as well as across HP_1, are substantially higher for the geometry with balconies than for the round roof or pitched roof geometries.

In the methodology used here for PC calculations, it is important to reiterate that only passenger vehicle emissions have been considered. Heavy duty transport has not been taken into account. Also emissions from households have not been considered. Therefore, for a comprehensive study of CO emissions, a more detailed emission source estimation would need to be performed, and ventilation efficiencies need to be quantified more accurately.

6 Conclusions

Mean flow and turbulence in an urban street canyon have been studied to understand the effect of variations in building geometries on street ventilation. The Air Exchange Rate (*ACH*) has been computed for two planes within the urban street canyon, one located at the building-top level and the second just above the pedestrian level. Direct LES estimations ACH_{LES} have been performed and the differences between the studied geometries analyzed. The results show that the round geometry is the one that most favourably promotes urban ventilation, while on the contrary the geometry with the façade with balconies is the one that most severely compromises urban ventilation. The building geometry with the round roof creates over two times larger exchanges than the one with balconies below HP_1 (the plane passing through the vertices of the buildings) and 5 times larger below HP_2 (the pedestrian level air exchange plane at 0.2 times the building height). Therefore, the study has shown that roof and façade geometries strongly influence the air exchanges between the street canyon and the free stream flows. Based on the ACH_{LES} estimate, the Pollutant Concentration (PC) within the canyon can be computed for the different building geometries. A two-reservoir model was developed and applied to compute these pollutant concentrations at the pedestrian level C_p (Below HP_2) and in the the canyon core C_c (between HP_1 and HP_2) for an illustrative example of carbon monoxide vehicular emissions; it shows similar trends with building geometry as those observed for the ACH_{LES} estimates, with rounder and smoother walls promoting more exchanges. The ventilation efficiency of a given geometry however plays a role in the actual ventilation; this requires further analysis using simulations that resolve the budget of the pollutant mass.

A novel formulation to compute the *ACH* has been proposed using data of mean vertical velocity and σ_w. This method, based on a folded normal distribution model of the vertical velocity, seeks to reduce the computational requirements so that *ACH* calculations can be performed with results obtained from RANS models with closures that provide σ_w. The comparisons between the direct LES results ACH_{LES} and the folded normal distribution estimates ACH_{FND} show a very good agreement with mean errors of less 2%, and maximum errors of around 4%. This is a significant improvement over two alternatively previous formulations that were tested here. Therefore, the results obtained from the folded normal distribution model provide a good approximation to the direct LES results, and can be used as a computationally less-demanding alternative that can use σ_w and the temporal and spatial mean of the vertical velocity $\langle \overline{w} \rangle$ obtained through RANS simulations.

Some of the limitations of the study are related to the assumed idealized deep street canyon building configurations with extruded 2-dimensional section profiles (with uniform building heights and aligned facades). In real urban configurations, building profiles generally vary along the longitudinal axis of the street canyon, and the later has a finite length. Furthermore, the approach flow angle of attack has been constrained to perpendicular to the street canyon axis. Isothermal conditions have also been imposed and thus surface heating or cooling was not considered, but it will have appreciable impact on the results. Therefore, while the results obtained can help us develop an understanding of the role that street canyon geometry plays in street ventilation, a complete picture of how flow and ventilation behave in realistic heterogeneous urban configurations, where 3-dimensional flow dynamics are significant, remains to be developed.

Acknowledgement

The authors thank the National Oceanographic and Atmospheric Administration's (NOAA) via the Cooperative Institute for Climate Science (CICS) of Princeton University and the Chair of Structural Design of the Institute of Technology and Architecture, ETH Zurich for their financial support. Elie Bou-Zeid is also supported by the US National Science Foundation's Sustainability Research Network Cooperative Agreement 1444758 and grant # ICER 1664091.

References

Anderson, W., Li, Q., Bou-Zeid, E., 2015. Numerical simulation of flow over urban-like topographies and evaluation of turbulence temporal attributes. Journal of Turbulence 16, 809-831.

ANSYS, 2013. ANSYS Fluent Theory Guide. Release 15.0. Ansys, Inc., Canonsburg, PA.

Aynsley, R.M., 1999. Shape and Flow: The Essence of Architectural Aerodynamics. Architecture Science Review 42, 69-74.

Barlow, J.F., Belcher, S.E., 2002. A Wind Tunnel Model for Quantifying Fluexes in the Urban Boundary Layer. Boundary-Layer Meteorology 104, 131-150.

Barlow, J.F., Harman, I.N., Belcher, S.E., 2004. Scalar Fluxes from Urban Street Canyons Part I: Laboratory Simulation. Boundary-Layer Meteorology 88, 279-306.

Bou-Zeid, E., 2005. Large Eddy Simulation of Atmospheric Boundary Layer Flow over Heterogeneous Surfaces. Johns Hopkins University, Baltimore, Maryland.

Bou-Zeid, E., Overney, J., Rogers, B.D., Parlange, M.B., 2009. The Effects of Building Representation and Clustering in Large-Eddy Simulations of Flows in Urban Canopies. Boundary-Layer Meteorology 132, 415-436.

Britter, R.E., Hanna, S.R., 2003. Flow and Dispersion in Urban Areas. Annual Review of Fluid Mechanics 35, 469-496.

Brown, M.J., Lawson, R.E., DeCroix, D.S., Lee, R.L., 2000. Mean Flow and Turbulence Measurements around a 2-D Array of Buildings in a Wind Tunnel, Conf. Appl. of Air Pollut. Meteorol.,11th. Am.Meteorol.Soc., Long Beach, Calif.

Buccolieri, R., Salizzoni, P., Soulhac, L., Garbero, V., Di Sabatino, S., 2015. The Breathability of Compact Cities. Urban Climate 13, 73-93.

Buccolieri, R., Sandberg, M., Di Sabatino, S., 2010. City Breathability and Its Link to Pollutant Concentration Distribution within Urban-Like Geometries. Atmospheric Environment 44, 1894-1903.

Cheng, W.C., Liu, C.H., Leung, D.Y.C., 2008. Computational Formulation for the Evaluation of Street Canyon Ventilation and Pollutant Removal Performance. Atmospheric Environment 42, 9041-9051.

Cheng, W.C., Liu, C.H., Leung, D.Y.C., 2009. On the Correlation of Air and Pollutant Exchange for Street Canyons in Combined Wind-Buoyancy-Driven Flow. Atmospheric Environment 43, 3682-3690.

Dezső-Weidinger, G., Stitou, A., Van Beeck, J., Riethmuller, M.L., 2003. Measurement of the Turbulent Mass Flux with PTV in a Street Canyon. Journal of Wind Engineering and Industrial Aerodynamics 91, 1117-1131.

Di Sabatino, S., Buccolieri, R., Pulvirenti, B., Britter, R.E., 2008. Flow and Pollutant Dispersion in Street Canyons Using FLUENT and ADMS-Urban. Environmental Modeling & Assessment 13, 369-381.

Di Sabatino, S., Solazzo, E., Paradisi, P., Britter, R., 2007. A Simple Model for Spatially-Averaged Wind Profiles Within and Above an Urban Canopy. Boundary-Layer Meteorology 127, 131-151.

EPA, 2008. Average Annual Emissions and Fuel Consumption for Gasoline-Fueled Passenger Cars and Light Trucks. Office of Transportation and Air Quality. Environmental Protection Agency, Washington.

EPA, 2010. Quantitative Risk and Exposure Assessment for Carbon Monoxide - Amended U.S. Environmental Protection Agency Office of Air Quality Planning and Standards Health and Environmental Impacts Division North Carolina.

EPA, 2014. Greenhouse Gas Emissions from a Typical Passanger Vehicle. Office of Transportation and Air Quality. Environmental Protection Agency, EPA.

Giometto, M., Christen, A., Meneveau, C., Fang, J., Krafczyk, M., Parlange, M., 2016. Spatial Characteristics of Roughness Sublayer Mean Flow and Turbulence Over a Realistic Urban Surface. Boundary-Layer Meteorol 160, 425-452.

Hamlyn, B., Britter, R.E., 2005. A Numerial Study of the Flow Field and Exchange Processes within a Canopy of Urban-Type Roughness. Atmospheric Environment 39, 3243-3254.

Hang, J., Sandberg, M., Li, Y., 2009. Age of Air and Air Exchange Efficiency in Idealized City Models. Building and Environment 44, 1714-1723.

Howard, L., 1838. The Climate of London, Deduced from Meteorological Obserbations Made at Different Places in the Neighbourhood of the Metropolis. C.Baldwin Printer, London.

Huang, Y., Hu, X., Zeng, N., 2009. Impact of Wedge-Shaped Roofs on Airflow and Pollutant Dispersion Inside Urban Street Canyons. Building and Environment 44, 2335-2347.

Hunter, L.J., Watson, I.D., Johnson, G.T., 1990. Modelling Air Flow Regimes in Urban Canyons. Energy and Buildings 15-16, 315-324.

Inagaki, A., Castillo, M.C.L., Yamashita, Y., Kanda, M., Takimoto, H., 2012. Large-Eddy Simulation of Coherent Flow Structures within a Cubical Canopy. Boundary-Layer Meteorology 142, 207-222.

Ingram, G.K., Liu, Z., 1999. Determinants of Motorization and Road Provision. Policy Research Working Papers, World Bank Group.

Kastner-Klein, P., Berkowicz, R., Britter, R., 2004. The Influence of Street Architecture on Flow and Dispersion in Street Canyons. Meteorology and Atmospheric Physics 87, 121–131.

Kastner-Klein, P., Plate, E.J., 1999. Wind-Tunnel Study of Concentration Fields in Street Canyons. Atmospheric Environment 33, 3973-3979.

Kellnerova, R., Kukacka, L., Jurcakova, K., Uruba, V., Janour, Z., 2012. PIV Measurement of Turbulent Flow Within a Street Canyon: Detection of Coherent Motion. Journal of Wind Engineering and Industrial Aerodynamics 104-106, 302-313.

Landsberg, H.E., 1981. The Urban Climate. Academic Press, New York.

Leone, F.C., Nelson, L.S., Nottingham, R.B., 1961. The Folded Normal Distribution. Technometrics 3, 543-550.

Li, Q., Bou-Zeid, E., Anderson, W., Grimmond, S., Hultmark, M., 2016. Quality and Reliability of LES of Convective Scalar Transfer at High Reynolds Numbers. International Journal of Heat and Mass Transfer 102, 959-970.

Li, X.X., Liu, C.H., Leung, D.Y.C., 2005. Development of a K-epsilon Model for the Determination of Air Exchange Rates for Street Canyons. Atmospheric Environment 39, 7285-7296.

Liu, C., Leung, D., Barth, M., 2005. On the Prediction of Air and Pollutant Exchange Rates in Street Canyons of Different Aspect Ratios Using Large-Eddy Simulation. Atmospheric Environment 39, 1567–1574.

Llaguno-Munitxa, M., Bou-Zeid, E., Hultmark, M., 2017. The influence of building geometry on street canyon air flow: Validation of large eddy simulations against wind tunnel experiments. Journal of Wind Engineering and Industrial Aerodynamics 165, 115-130.

Moonen, P., Dorer, V., Carmeliet, J., 2011. Evaluation of the Ventilation Potential of Courtyards and Urban Street Canyons using RANS and LES. Journal of Wind Engineering and Industrial Aerodynamics 99, 414-423.

Nazarian, N., Martilli, A., Kleissl, J., 2017. Impacts of Realistic Urban Heating, Part I: Spatial Variability of Mean Flow, Turbulent Exchange and Pollutant Dispersion. Boundary-Layer Meteorology, 1-27.

Neophytou, M.K.A., Britter, R.E., 2005. Modelling the Wind Flow in Complex Urban Topographies: a Computational-Fluid-Dynamics Simulation of the Central London Area, Fifth GRACM International Congress on Computational Mechanics, Limassol, Cyprus.

Ng, E., 2009. Policies and technical guidelines for urban planning of high-density cities – air ventilation assessment (AVA) of Hong Kong. Building and Environment 44, 1478-1488.

Ng, E., 2012. Towards planning and practical understanding of the need for meteorological and climatic information in the design of high-density cities: A case-based study of Hong Kong. International Journal of Climatology 32, 582-598.

NYSDOT, 2011. New York State Department of Transportation. 2011 Traffic Data Report for New York State, New York.

Oke, T.R., 1987. Boundary Layer Climates. Methuen & Co. Ltd, York, UK.

Oke, T.R., 1988a. Street Design and Urban Canopy Layer Climate. Energy and Buildings 11, 103-113.

Oke, T.R., 1988b. The Urban Energy Balance. Progress in Physical Geography 12, 471-508.

Panagiotou, I., Nophytou, M.K.A., Hamlyn, B., Britter, R.E., 2013. City breathability as quantified by the exchange velocity and its spatial variation in real inhomogeneous urban geometries: An example from central London urban area. Science of the Total Environment 442, 466–477.

Piomelli, U., Moin, P., Ferziger, J.H., 1988. Model Consistency in Large Eddy Simulation of Turbulent Channel Flows. Physics of Fluids 31, 1884-1891.

Poggi, D., Katul, G.G., 2008. Micro and macro disperisve fluxes in canopy flows. Acta Geophys 56, 778-799.

Pope, S.B., 2000. Turbulent flows. Cambridge University Press, New York.

Rafailidis, S., 1997. Influence of Building Areal Density and Roof Shape on the Wind Characteristics Above a Town. Boundary-Layer Meteorology 85, 255-271.

Rafailidis, S., Schatzmann, M., 1996. Physical Modeling of Car Exhaust Dispersion in Urban Street Canyons. The Effect of Slanted Roofs. Air Pollution Modelling and its Application XI.

Ramponi, R., Blocken, B., de Coo, L.B., Janssen, W.D., 2015. CFD Simulation of Outdoor Ventilation of Generic Urban Configurations with Different Urban Densities and Equal and Unequal Street Widths. Building and Environment 92, 152-166.

Raupach, M.R., Shaw, R.H., 1982. Averaging Procedures for Flow Within Vegetation Canopies. . Boundary-Layer Meteorology 22, 79-90.

Riain, C.M.N., Fisher, B., Martin, C.J., Littler, J., 1998. Flow Field and Pollution Dispersion in a Central London Street. Environment Monitoring and Assessment 52, 299-314.

Salizzoni, P., Marro, M., Soulhac, L., Grosjean, N., Perkins, R.J., 2011. Turbulent Transfer Between Street Canyons and the Overlying Atmospheric Boundary Layer. Boundary-Layer Meteorology 141, 393-414.

Salizzoni, P., Soulhac, L., Mejean, P., 2009. Street Canyon Ventilation and Atmospheric Turbulence. Atmospheric Environment 43, 5056-5067.

Shur, M.L., Spalart, P.R., Strelets, M.K., Travin, A.K., 2008. A hybrid RANS-LES approach with delayed-DES and wall-modelled LES capabilities. International Journal of Heat and Fluid Flow 29, 1638-1649.

Slotnick, J., A. Khodadoust, J. Alonso, D. Darmofal, W. Gropp, E. Lurie, Mavriplis, D., 2014. CFD Vision 2030 Study. NASA, Langley Research Center, Hampton, Virginia

Smagorinsky, J., 1963. General Circulation Experiments with the Primitive Equations, in: James E.Caskey, J. (Ed.), Montly Weather Review. Weather Bureau, Washington D.C.

Solazzo, E., Britter, R.E., 2007. Transfer Processes in a Simulated Urban Street Canyon. Boundary-Layer Meteorology 124, 43-60.

Takano, Y., Moonen, P., 2013. On the Influence of Roof Shape on Flow and Dispersion in an Urban Street Canyon. Journal of Wind Engineering and Industrial Aerodynamics 123, 107-120.

Temmerman, L., Leschziner, M.A., Mellen, C., Fröhlich, J., 2003. Investigation of Subgrid-Scale Models and Wall-Function Approximations in Large Eddy Simulation of Separated flow in a Channel with Streamwise Periodic Constrictions. International Journal of Heat and Fluid Flow 24, 157-180.

Theodoridis, G., Moussiopoulos, N., 2000. Influence of Building Density and Roof Shape on the Wind and Dispersion Characteristics in an Urban Area. A numerical study. Environmental Monitoring and Assessment 65, 407–415,.

Tominaga, Y., 2012. Visualization of city breathability based on CFD technique: case study for urban blocks in Niigata City. Journal of Visualization 15, 269-276.

Transport of London, 2015. Low Emission Zone. https://tfl.gov.uk/modes/driving/low-emission-zone. Accessed 15th of June 2016.

UNFPA, 2014. Population and Sustainable Development in the Post-2015 Agenda, p. 56.

Vardoulakis, S., Fisher, B.E.A., Pericleous, K., Gonzalez-Flesca Hernandez, N., 2003. Modelling air quality in street canyons: a review. Atmospheric Environment 37, 155-182.

WHO, 2014. World Urbanization Prospects 2014. United Nations.

Xie, X., Huang, Z., Wang, J., Xie, Z., 2005. The Impact of Solar Radiation and Street Layout on Pollutant Dispersion in Street Canyon. Building and Environment 40, 201-212.

Xie, X., Liu, C.H., Leung, D.Y.C., Leung, M.K.H., 2006. Characteristics of Air Exchange in a Street Canyon with Ground Heating. Atmospheric Environment 40, 6396-6409.

Xie, Z.T., Castro, I.P., 2009. Large-Eddy Simulation for Flow and Dispersion in Urban Streets. Atmospheric Environment 43, 2174-2185.

Yaghoobian, N., Kleissl, J., Paw, U.K.T., 2014. An Improved Three-Dimensional Simulation of the Diurnally Varying Street-Canyon Flow. Boundary-Layer Meteorology 153, 251-276.

Yassin, M.F., 2011. Impact of Height and Shape of Building Roof on Air Quality in Urban Street Canyons. Atmospheric Environment 45, 5220-5229.